



HAL
open science

Heavy-ion Irradiations of Fe and Fe-Cr Model Alloys Part 1: Damage evolution in thin-foils at lower doses

Zhongwen Yao, Mercedes Hernández-Mayoral, Mike Jenkins, Mark Kirk

► **To cite this version:**

Zhongwen Yao, Mercedes Hernández-Mayoral, Mike Jenkins, Mark Kirk. Heavy-ion Irradiations of Fe and Fe-Cr Model Alloys Part 1: Damage evolution in thin-foils at lower doses. *Philosophical Magazine*, 2008, 88 (21), pp.2851-2880. 10.1080/14786430802380469 . hal-00513952

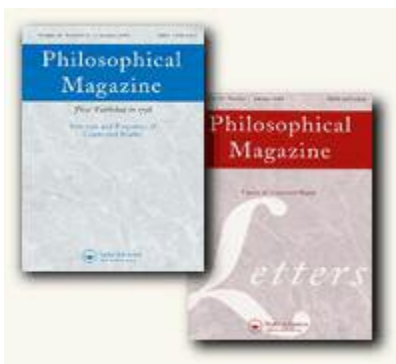
HAL Id: hal-00513952

<https://hal.science/hal-00513952>

Submitted on 1 Sep 2010

HAL is a multi-disciplinary open access archive for the deposit and dissemination of scientific research documents, whether they are published or not. The documents may come from teaching and research institutions in France or abroad, or from public or private research centers.

L'archive ouverte pluridisciplinaire **HAL**, est destinée au dépôt et à la diffusion de documents scientifiques de niveau recherche, publiés ou non, émanant des établissements d'enseignement et de recherche français ou étrangers, des laboratoires publics ou privés.



**Heavy-ion Irradiations of Fe and Fe-Cr Model Alloys
Part 1: Damage evolution in thin-foils at lower doses**

Journal:	<i>Philosophical Magazine & Philosophical Magazine Letters</i>
Manuscript ID:	TPHM-08-Feb-0046.R1
Journal Selection:	Philosophical Magazine
Date Submitted by the Author:	15-Jul-2008
Complete List of Authors:	Yao, Zhongwen; University of Oxford, Materials Hernández-Mayoral, Mercedes; CIEMAT, Division of Materials Jenkins, Mike; University of Oxford, Materials Kirk, Mark; Argonne National Laboratory, Materials Science
Keywords:	in-situ electron microscopy, radiation damage
Keywords (user supplied):	FeCr alloys
<p>Note: The following files were submitted by the author for peer review, but cannot be converted to PDF. You must view these files (e.g. movies) online.</p> <p>video 1 paper 1.mpg video 2 paper 1 .mpg video 3 paper 1.mpg video 4 paper 1.mpg video 5 paper 1.mpg video6.mov</p>	



Heavy-ion Irradiations of Fe and Fe-Cr Model Alloys

Part 1: Damage evolution in thin-foils at lower doses

Z. Yao^{*}, M. Hernández-Mayoral^{**}, M. L. Jenkins^{*1} and M. A. Kirk^{***}

^{*} Department of Materials, University of Oxford, Parks Rd., OX1 3PH

^{**} Division of Materials, CIEMAT Avenida Complutense, 22, 28040-Madrid

^{***} Materials Science Division, Argonne National Laboratory, Argonne, IL 60439

For Peer Review Only

¹ Corresponding author: Email: mike.jenkins@materials.ox.ac.uk

Abstract

The evolution of radiation damage in Fe and FeCr alloys under heavy-ion irradiation has been investigated by TEM. Thin foils were irradiated with 100 or 150 keV Fe⁺ and Xe⁺ ions at room temperature and 300°C. Dynamic observations followed the evolution of damage. We report on early stages in damage development. Small (2-5 nm) dislocation loops first appeared at doses between 10¹⁶ and 10¹⁷ ions m⁻² in all materials. Loop number densities depended strongly on the foil orientation in pure Fe but not in FeCr alloys. Number densities did not depend strongly on Cr content. For a given material, defect yields were higher for Xe⁺ ions than for Fe⁺ ions, and were higher at RT than at 300°C. Loops with both <100> and ½ <111> Burgers vectors were identified. The proportion of <100> loops was larger, especially in pure Fe. Dynamic observations showed that: (1) the contrast of some new loops developed over intervals as long as 0.2s; (2) hopping of ½ <111> loops was induced by the ion and electron beams and was pronounced in ultra-pure iron; and (3) many loops were lost during and after ion irradiation by glide to the foil surface. The number of loops retained was strongly dependent on the foil orientation in Fe, but less so in FeCr alloys. This is due to a lower loop mobility in FeCr alloys probably due to pinning by Cr atoms. Reduced loop loss probably explains the lower loop number densities in FeCr alloys compared with pure Fe.

Deleted: specimens

Deleted: heavy

Deleted: here

Deleted: The threshold dose for visible damage in Fe-Cr alloys was lower than in pure Fe irradiated under the same conditions and loop number densities at a given dose were higher.

Deleted: that

Deleted: loop motion

Deleted: particularly

Deleted: that

Deleted: and probably explains the lower number densities of loops in thin foils

Deleted: of Fe

Keywords: radiation damage, FeCr alloys, *in-situ* TEM

§1 Introduction and background

Fusion and Generation IV fission reactors are promising candidates for future power generation. The rapid and successful development of these energy sources requires a fundamental understanding of radiation damage in materials located in regions of high neutron flux, including the development of robust models with predictive capability. For this reason there has recently been a renewed interest in radiation damage mechanisms in ferritic materials, which are likely to form the basis of most structural materials used in these reactors. Low-activation ferritic/martensitic steels, typically containing about 9% Cr and smaller quantities of W, V and Ta, such as EUROFER 97, are regarded as potentially superior alternatives to austenitic steels because of their better thermal properties and higher swelling resistance [1-3]. However they exhibit low-temperature, irradiation produced hardening which may make their use problematic at temperatures below 400°C. The hardening is believed to be due to the accumulation of radiation damage. Radiation damage mechanisms in these complex materials are not well understood. At present it is not clear how to modify existing steels so that they would adequately withstand the demanding fusion reactor environment, or even whether this is possible.

Deleted: ¶

Deleted: For example, the most promising candidate materials for structural applications in fusion reactors are 1

Deleted: -12

Deleted: JLF, F82H, OPTIMAX and more recently

Deleted: . These

Fundamental aspects of radiation damage can often be better understood by investigating pure materials and simple model alloys. This is the approach adopted in our work. In addition multi-scale modeling is increasingly being used to predict the evolution of microstructures under irradiation, and in order to achieve a benchmarked modeling capability, validation-oriented experiments are required. The work described in this paper was carried out under the auspices of two such modeling programs. These include a UK program led by [the University of Oxford](#) which is focused on irradiation effects and mechanical properties in materials for future fusion reactors and the European PERFECT program, which is devoted to the development of multiscale numerical tools for simulating the effects of irradiation on mechanical and corrosion properties of materials used in existing fission nuclear power plants. In this and the following paper we report results on radiation damage development in thin foils of model Fe and Fe-Cr alloys under heavy-ion irradiations aimed at gaining a better fundamental understanding of radiation damage in [ferritic](#) materials.

Deleted: fission- and fusion-relevant

Under neutron irradiation, most atomic displacements in metals take place within cascades generated by energetic primary knock-on atoms, with typical energies of several tens of keV. The vacancy-rich cores of individual cascade regions may in some cases spontaneously collapse to form vacancy dislocation loops. Such loops are generally thought to form in the “thermal-spike” phase of the cascade in a time of around 10^{-11} seconds. Cascade collapse has usually been investigated in experiments where electron-transparent thin foils are irradiated with heavy-ions, which are then examined in a transmission electron microscope (TEM). In experiments with self-ions the ions mimic the primary knock-ons produced by neutrons. By controlling the energy and mass of the incident ions, cascade parameters such as the cascade volume and energy density can be varied, allowing cascade collapse to be studied systematically. Molecular dynamics simulations indicate that interstitial clusters may also be formed directly in displacement cascades e.g. [4]. In thin-foil irradiations however, the interstitial component of the damage may not be seen, at least at low doses, since interstitials and small interstitial clusters are probably highly mobile and most will be lost to the foil surfaces. There is however good reason to believe that data on cascade collapse obtained in thin-foil experiments is relevant to cascades created in the bulk by neutron irradiation [5].

Thin-foil heavy-ion irradiations have now been performed on a wide variety of metals and alloys (for reviews see [6-7]). In low-dose self ion irradiations of pure copper it is found that for ion energies greater than about 30keV the defect yield (defined as the number of visible clusters per incident ion) is close to unity, that is, vacancy loops are produced in most cascades. High defect yields are found in many other metals and alloys. However, in pure iron cascade collapse takes place much less readily if at all. Irradiation of thin foils of high-purity Fe with 40-240 keV self-ions to low doses ($< 10^{16}$ ions m^{-2}) at room temperature (RT) resulted in no visible damage [8]. Irradiation with ions heavier than Ga^+ (which produce more compact cascades than self-ions) resulted in a low yield of vacancy-type dislocation loops with Burgers vectors $\mathbf{b} = \frac{1}{2} \langle 111 \rangle$ or $\langle 100 \rangle$. For 80 keV W^+ ions, the two types of loops occurred in approximately equal numbers. The defect yield is a strong function of the ion mass, and is very low for relatively light ions such as Ga^+ and reaches a true value close to unity for 80keV W^+ ions (when account is taken of $\mathbf{g} \cdot \mathbf{b} = 0$ contrast invisibility and the loss of glissile loops to the surface, see [8]).

Although collapse of individual, isolated cascades in Fe does not occur under self-ion irradiations, visible damage is seen at high ion doses. Robertson *et al* [9] reported the formation of loops in {110} foils of Fe under 50 keV and 100 keV self-ion irradiation at 40K carried out *in-situ* in the former Argonne-HVEM Facility. In 100 keV irradiations, loops first appeared at a dose of 8×10^{16} ions m^{-2} . The loop density then increased non-linearly up to at least 8×10^{17} ions m^{-2} . Similar trends were found in 50 keV irradiations. The specimens were observed as they warmed from 40K to RT. An increase in loop number density of about 30% was seen. This was attributed to the appearance of a population of small ($< 4nm$) loops, which outweighed the disappearance of a few loops. A few loops were also seen to grow on warming. In a Burgers vector analysis of a specimen irradiated with 50 keV ions, carried out at room temperature after warming, the majority (about 80%) of the analyzable loops were found to have Burgers vectors $\mathbf{b} = \frac{1}{2} \langle 111 \rangle$ whilst the remainder had $\mathbf{b} = \langle 100 \rangle$. Of the loops present after warm-up, several could be traced back to micrographs taken at 40K and all of these had $\mathbf{b} = \frac{1}{2} \langle 111 \rangle$. The habit planes of the $\frac{1}{2} \langle 111 \rangle$ loops varied from pure-edge {111} to close to {110}, suggesting that loops had nucleated on {110} planes according to the Eyre-Bullough mechanism [10].

Deleted: ² (which was the maximum dose used by these authors at this ion energy)

Deleted: In

Deleted: a similar trend was found, although the onset of damage occurred at a higher dose, and the loop density at a given dose was about an order of magnitude lower than for 100 keV ions

Deleted: The slope of the log-log plot of loop density versus dose was about 1.5 in both cases

Robertson *et al* [9] were not able to determine the vacancy or interstitial nature of the loops. On the basis of previous heavy-ion experiments they thought the loops were more likely vacancy in nature. They considered that the loops were not formed by the direct collapse of individual, isolated cascades. However, since 40K is below Stage I in Fe, neither could the loops have been produced by long-range diffusion, nucleation and growth processes. Instead it was concluded that the formation of vacancy loops in cascades produced by self-ions requires that two or more cascades overlap spatially. This conclusion is consistent with the observation that loops are first seen at doses $> 10^{16} m^{-2}$ when cascade overlap becomes significant. Such a mechanism had also been postulated by Dunlop *et al* [11] to explain their electrical resistivity experiments in iron neutron-irradiated at 4.2K. Recent molecular dynamics simulations suggest that small, sub-microscopic vacancy clusters (as well as small, mobile interstitial clusters) are produced in individual cascades in Fe [12]. Robertson *et al*'s observations of the appearance and growth of loops on warming from 40K to RT are also consistent with the presence of sub-microscopic vacancy clusters in uncollapsed or partially-collapsed cascades. These vacancy clusters may take the form of small voids according to recent atomistic simulations by Gilbert *et al* [13], which suggest that in Fe small spherical voids are more stable than vacancy dislocation loops for clusters of any size, and planar voids (effectively uncollapsed discs of vacancies) are more stable than dislocation loops for sizes up to about 3 nm. As the irradiation proceeds it would be expected that the

background density of such relatively immobile vacancy clusters would increase. It was speculated that a visible loop could be formed when a second cascade (or sub-cascade) is produced at the site of an earlier cascade, with vacancies from both cascades participating in a collapse mechanism similar to that which occurs in individual cascades in other metals. In subsequent experiments, Kirk *et al* [14] showed that dislocation loops are also produced at room temperature at overlap doses in self-ion irradiations of Fe. Loops were first seen at a dose of about $6 \times 10^{17} \text{ m}^{-2}$ for 100 keV ions.

Heavy-ion damage in Fe-Cr alloys and ferritic/martensitic steels has not previously been investigated extensively. Fukushima *et al.* [15] have reported a study of heavy-ion damage in an Fe-9%Cr ferritic steel and a Japanese Ferrite Martensitic Steel (JFMS). These authors irradiated thin foils of these materials with 40 keV Cu^+ and Fe^+ ions to doses of $8 \times 10^{16} - 8 \times 10^{17} \text{ ions m}^{-2}$ at RT. Defect clusters in the form of small (1-3nm) white dots in weak-beam images, believed to be dislocation loops, were observed. The defect yields in both materials were low (<0.01) again suggesting that cascade overlap was necessary for collapse to occur, as in pure Fe. The authors considered that about 90% of the loops were vacancy and 10% interstitial, but their use of the 2 1/2-D technique may make this conclusion unreliable [16].

In the present paper and the following paper we revisit thin-foil ion irradiation experiments in pure Fe and extend these experiments to FeCr binary alloys, which form the basis of reduced activation steels and which are the subject of an intense modeling effort. We make particular use of the enhanced capabilities of the Argonne IVEM-Tandem Facility for *in-situ* ion irradiation experiments, which allowed us to follow dynamically the evolution of radiation damage microstructures over a larger dose range and at better resolution than in previous experiments. In this paper we describe damage evolution under heavy-ion irradiation in various grades of pure Fe and several FeCr alloys at doses $\leq 2 \times 10^{18} \text{ ions m}^{-2}$ (and in one dynamic experiment $\sim 4 \times 10^{18} \text{ ions m}^{-2}$ for comparison purposes, §3.6.2). We pay particular attention to the effect of Cr on damage evolution, since the Cr content of steels and FeCr alloys is known to affect both fracture behaviour and void swelling. The minimum change in DBTT occurs at a Cr content of about 9% [2]. Void swelling is a minimum between 5-10%Cr [17]. We also describe two dynamic observations. The first is the "hopping" of small loops produced in thicker regions of foil in the early stages of irradiation, especially in UHP iron. The second is an unexpected time dependence of the formation of individual loops whereby the contrast of some newly-formed loops increased over times as long as 0.2s before saturating. We postpone to Part 2 a detailed presentation and discussion of the complex microstructures which develop in thicker areas of foil at higher doses.

§2. Experimental details

Both polycrystalline and single-crystal materials were investigated. Ultra-high purity (UHP) iron was available in polycrystalline form and contained ~1ppm C, < 5ppm N, < 10ppm Si and very small quantities of other impurities. Polycrystalline iron of lower (5N) purity was also available (so-called "Hawthorne" alloy 1A, containing about 0.01 wt% impurities including 0.013wt%C, see reference [18] for the full composition). Single crystal iron (99.99+%, 4N+) was provided by Metal Crystals and Oxides Ltd., Cambridge. The FeCr alloys were also manufactured by the same company from starting materials of purity 99.99+% and included Fe-Cr (5, 8, 11 wt.%) polycrystalline alloys and Fe-Cr (9, 18wt.%) single crystal alloys. The polycrystalline materials were supplied as cold-rolled foil of thickness 0.1 ~ 0.3 mm. The single crystals of Fe and FeCr were cut into slices with a <100> normal by spark erosion.

Deleted: more likely

Deleted: ¶

Deleted: The slope of the log-log graph of loop density versus dose in this case was 0.7. The difference in slope at 30K and RT has never been fully explained.¶

Deleted: was

Deleted: ¶

. There have been a number of studies of damage development in bulk FeCr alloys under neutron irradiation. Gelles [17] carried out neutron irradiations of a range of FeCr alloys (0-12%Cr) at 400°C to 15 displacements per atom (dpa) and found populations of loops, probably of interstitial type, and in most alloys voids. The loops in low (e.g 3%) Cr alloys had predominantly <100> Burgers vectors, whilst the loops in higher Cr alloys (e.g. 12%) were a mix of <100> and 1/2<111> types. He suggested that this correlated with the strong swelling suppression of low Cr alloys. Parollo *et al* [18] reported results on neutron irradiations of Fe-Cr alloys with various additions of Cr ranging from 0 to 18%. Specimens were irradiated in bulk at 400°C to doses of 5.5 -7.1 dpa. Again, dislocation loops with Burgers vectors <100> and 1/2<111> were observed. Cr additions in alloys again resulted in increases in the fractions of loops with $b = 1/2<111>$. Konobeev *et al* [19] investigated swelling and microstructure of pure Fe and Fe-... [1]

Formatted: Font color: Red

Formatted: Font color: Blue

Deleted: 22

Deleted: report

Deleted: new

Formatted: Font color: Auto

Deleted: extreme mobility

Formatted: Font color: Auto

Deleted:

Formatted: Font color: Auto

Deleted: whereby

Formatted: Font color: Auto

Formatted: Font color: Auto

Formatted: Font color: Auto

Deleted:

Formatted: Font color: Blue

Formatted: Heading 1

Deleted: ¶

Deleted: 23

The as-received foils and single-crystal slices were first thinned to less than 0.15 mm by mechanical polishing. Standard 3mm TEM discs were then punched and these were further thinned mechanically to a thickness 50 ~ 100 μm . The dislocation density in the discs was reduced by annealing in vacuum at 800 $^{\circ}\text{C}$ for an hour followed by slow cooling. After this treatment all specimens had a simple ferritic microstructure with a low dislocation density.

The discs were then electro-polished into TEM thin foils, using an electrolyte of 5% perchloric acid plus 95% methanol at low temperature -60 $^{\circ}\text{C}$. The samples were washed successively in cold methanol (-60 $^{\circ}\text{C}$), methanol and ethanol. The polished samples were introduced immediately into the microscope if possible, in some cases under a nitrogen atmosphere as this was found to improve the surface quality. If specimens could not be introduced into the microscope immediately, they were stored either in water-free ethanol or in vacuum. Only specimens with high-quality surfaces were chosen for analysis. Although it was generally easier to produce high-quality specimens of FeCr alloys than of pure Fe, the best specimens of all materials were comparable and allowed dislocation loops of size $\sim 2\text{nm}$ to be imaged. Details of the specimen preparation procedure are given in [19].

In-situ experiments were carried out at the IVEM-Tandem Facility at Argonne National Laboratory. The Facility consists of a Hitachi H-9000NAR transmission electron microscope interfaced to a 2 MV tandem ion accelerator and a 0.65 MV ion implanter [20]. Only the ion implanter was used in the present experiments. Foils of the different materials were mounted in a double-tilt holder and irradiated at room temperature (RT) or 300 $^{\circ}\text{C}$ with 100keV or 150 keV Fe^{+} or 100 keV Xe^{+} ions to maximum total doses ranging from a few 10^{18} ions m^{-2} to 2×10^{19} ions m^{-2} in several dose increments, with microscopy performed after each dose step. The dose rate was typically about 8×10^{14} ions $\text{m}^{-2} \text{s}^{-1}$. The accuracy of dose measurements is typically about $\pm 10\%$ (see Daulton *et al* [21] for a full discussion). Some experiments used as an irradiation source an FEI FIB, which produces 30keV Ga^{+} ions. The ion energies were chosen to mimic high-energy fusion neutron cascades and for comparison with earlier works (e.g. [6-9, 14]). The depths of the peak damage in Fe determined by SRIM calculations [22] for these different cases were 19 nm (100keV Fe^{+}), 28 nm (150keV Fe^{+}) 12 nm (100keV Xe^{+}) and 6 nm (30keV Ga^{+} ions) respectively.

SRIM calculations were also performed to determine doses in displacements per atom. For a minimum threshold displacement energy in Fe of 24 eV [23], it was found that a dose of 1×10^{19} 150 keV Fe^{+} ions m^{-2} gives a damage level of about 6.5 dpa over a range of foil thickness 15-45 nm. If we took instead an average displacement energy of about 40 eV [24] the dpa values quoted here would be about halved. In the present paper, where we concentrate on the early stages of damage evolution at doses $< 2 \times 10^{18} \text{m}^{-2}$, the maximum damage levels were $\sim 1\text{dpa}$.

All TEM observations were made at an operating voltage of 200 kV which is well below the threshold voltage for electron knock-on damage in Fe, using weak beam dark field (WBDF), kinematical bright-field (KBF) and dynamical two-beam diffraction conditions. In some *in-situ* experiments dynamic observations were made using a Gatan model 622C image-intensified video-rate fibre-optic coupled camera which writes images via an analogue to digital converter to a computer hard-drive for eventual DVD recording. This system allows the *in-situ* recording of images during and immediately after ion irradiation. This is possible with the ANL instrument because of the high angle

Deleted: 24

Deleted: Both *ex-situ* and *in-situ* experiments were performed on UHP Fe. In *ex-situ* experiments, specimens of UHP Fe were irradiated with 150 keV Fe^{+} ions at 300 $^{\circ}\text{C}$ in the CSNSM Facility in Orsay, France to doses from 10^{18} to 2×10^{19} ions m^{-2} at a dose rate of 4×10^{15} ions $\text{m}^{-2} \text{s}^{-1}$. They were returned to CIEMAT in Madrid for examination in a JEOL 2010 transmission electron microscope.

Deleted: on all materials

Deleted: 25

Deleted: s

Deleted:

Deleted: 26

Deleted: One

Deleted: at Oxford

Deleted: 27

Deleted: 28

Deleted: take

Deleted: 29

Deleted: will

Deleted: therefore

Deleted: ¶

¶

of incidence of the ion beam ($\sim 70^\circ$) which allows specimens to be viewed during ion irradiation without having to tilt them towards the beam.

In all experiments care was taken to maintain consistent imaging conditions (including foil orientation, diffraction vectors and deviation parameters) so that proper comparisons could be made of damage structures from one area to another of the same specimen at a given dose, or of the same area with increasing dose, or from one specimen to another. The polycrystalline specimens had a strong {111} texture, with grain sizes of several tens of μm . It was often the case that only grains with normals within several degrees of [111] were available for examination. Some experiments were done in grains of other orientations, e.g. (110), (112) and (113), if these were available, as stated in the text. Single-crystal (001) foils were used for Burgers vectors determinations (see §3.3). Number density and image size measurements were made from weak-beam micrographs recorded in $g = \bar{1}10$. In counting defects it was sometimes difficult to distinguish very small irradiation-produced loops from surface features. If such an ambiguity existed, the feature was counted as a half following our previous practice in work in Fe [14]. The error bars in number density were determined by the number of such loops as a proportion of the total. A full description of the experimental techniques can be found in ref [25].

§3 Results

3.1 Damage thresholds and loop number densities

The threshold doses for visible damage depended on material, ion, foil orientation and irradiation temperature but all fell in a range $10^{16} - 10^{17}$ ions m^{-2} . No damage was visible in either grade of pure Fe under any irradiation condition below a dose of about 2×10^{16} ions m^{-2} (~ 0.01 dpa). These threshold doses are about 2-3 orders of magnitude higher than in copper and several other metals irradiated under similar conditions, but similar to earlier results in Fe [6-9]. In all cases the damage initially took the form of small ($\sim 1-5$ nm) dislocation loops, which were visible as white dots in weak-beam images or as dark dots in KBF images. Figure 1 shows small dislocation loops in a (110) foil of UHP Fe and a (113) foil of Fe8%Cr, both irradiated with 150 keV Fe^+ ions to a dose of 5×10^{17} ions m^{-2} at RT. For these irradiation conditions the micrographs look very similar, with no obvious differences in loop number densities or sizes.

The accumulation of damage in different materials under different irradiation can best be compared by making measurements of loop numbers and size distributions as a function of dose. Thin-foil experiments at low doses are usually concerned with individual cascade events. In such experiments it is usual to measure the number of loops per unit area (the areal density) rather than the number per unit volume. In the present experiments (as well as in previous experiments on Fe) the ion doses are much higher such that spatial overlap of cascades occurs, and so we are probably not dealing with individual cascade events. In this case the use of areal densities must be justified. For example, at high doses loops may be produced by interstitial clustering in thicker areas, where the surface is not such a dominant sink (see Part 2). Figure 2 shows measured areal densities in pure Fe irradiated with 100keV Fe^+ ions at RT to a dose of 2×10^{18} m^{-2} , plotted as a function of the foil thickness. Clearly there is no trend for the areal density to increase over this range of foil thickness (15-85 nm) at this dose. The same was found to be true in other cases for doses less than 2×10^{18} ions m^{-2} . The gradual fall-off in number densities with foil thickness seen in Figure 2 is most likely due to a lower visibility

Deleted: of orientation

Deleted: These specimens were most commonly imaged under weak-beam conditions using a diffraction vector $g = \bar{1}10$ with the foil oriented close to (111).

Deleted: Other diffraction conditions

Deleted: 1

Deleted: 1

Deleted: 30

Deleted: 7

Deleted: kinematical

Deleted:

Deleted: a (110) foil of UHP Fe

Deleted: and

Deleted: in a

Deleted: at RT

Deleted: .

Deleted: ¶

Deleted: No damage was visible in either grade of pure Fe under any irradiation condition below a dose of about 2×10^{16} ions m^{-2} (~ 0.01 dpa). Figure 1 shows small dislocation loops in UHP Fe irradiated in an *ex-situ* experiment with 150 keV Fe^+ ions at 300°C to a dose of 1×10^{18} ions m^{-2} . The micrograph was taken under weak beam conditions, ($g = \bar{1}10$) using the reflection $g = \bar{1}10$ in a foil oriented close to (111).¶

Deleted: Figure 2 shows a series of images of the same area of a Fe-11... [2]

Deleted: and imaging conditions

Deleted: In

Deleted: t

Deleted: we are normally

Deleted: .

Deleted: The defect yield is ther... [3]

Deleted: 4

Deleted: The foil thickness was ... [4]

Deleted: with

Deleted: 5

Deleted: .

Deleted:

Deleted: about

Deleted:

Deleted: 10^{19}

of small loops in thick foils [26]. There were few defects in areas of foil of thickness $< 10\text{nm}$, consistent with the SRIM simulations for this irradiation condition.

Loop number densities are shown as a function of dose for a number of different materials and irradiation conditions in Figures 3(a) and (b). These measurements were made in foils of moderate thickness ($< 50\text{ nm}$) and have not been corrected for systematic absences (when dislocation loops are not seen because $\mathbf{g}\cdot\mathbf{b} = 0$) nor for loss of glissile loops to the surface (see §3.5 below). They were however made in regions of specimen which were remote from the area observed in video recordings, and so had not been exposed to electrons during ion irradiation (for reasons discussed below). Time and specimen constraints made it not feasible to explore all of parameter space, and so it was not always possible to identify trends with full confidence. However, for both pure Fe and FeCr alloys there was a trend for loop densities in a given material at a given dose to be higher for Xe^+ ions than for Fe^+ ions.

Figure 3(a) shows results for polycrystalline 5N and UHP Fe. Also shown on this plot are the earlier results of Kirk *et al* [14] which were obtained in {110} foils. The areal density of visible loops varied considerably between different materials and irradiation conditions. Differences in number density seemed not to be related to material purity, but some consistency is found if these differences are attributed to differences in grain orientation. Low number densities were recorded in foils of both UHP and 5N Fe with orientation close to (111) irradiated with Fe^+ ions. Number densities at other foil orientations for Fe^+ ion irradiation were much higher. Loop number densities N increased with dose ϕ at a rate $N = \phi^n$ with $n \approx 1$ for Xe^+ irradiation at RT and $n \approx 2$ for 100keV Fe^+ ions at RT.

Figure 3(b) shows results for room temperature irradiations of FeCr alloys. Some slopes are again indicated. All these measurements were made in foils of orientation close to (111). Loop number densities at the same dose for 100 keV Fe^+ irradiation were similar for the 5 and 8% Cr alloys and somewhat higher for the 11% Cr alloy. The number densities at the same dose in all cases were more than an order of magnitude higher than for 5N Fe of the same orientation irradiated under the same condition. For Fe^+ irradiations of all three alloys the slopes n are initially >1 but then decrease. In Xe^+ irradiation of Fe8%Cr, loops were seen at a relatively low dose but the number density increased only slowly with dose. There may be a tendency in all cases for the loop areal density to plateau at about 10^{15} loops m^{-2} .

In the *in-situ* experiments it was not possible to investigate systematically the effects of different foil orientations in FeCr alloys, because a majority of specimens were of orientation close to (111). Loop density measurements were however made for Fe11%Cr specimens of different orientations irradiated *ex-situ* with 30 keV Ga^+ ions in a FIB. Unlike the case for pure Fe, loop number densities did not depend on the foil orientation. Specimens with grains oriented close to (110), (111) and (113) were irradiated at the same time in the FIB to a dose of 5×10^{17} ions m^{-2} . In these three cases the measured loop densities were $1.03 \pm 0.2 \times 10^{15}$ loops m^{-2} , $1.14 \pm 0.2 \times 10^{15}$ loops m^{-2} and $0.96 \pm 0.2 \times 10^{15}$ loops m^{-2} respectively. These values are not considered to be significantly different.

Figure 4 shows data for Fe11%Cr which illustrate why it is important to distinguish between areas which were exposed to 200kV electrons during the ion irradiation and those which were not. Despite the fact that the electron energy is well below the threshold for knock-on displacement damage, it can be seen that the effect of simultaneous electron irradiation is to decrease the measured loop

Deleted: N

Deleted: 5

Deleted:

Deleted: F

Deleted: were

Deleted: general

Deleted: s

Deleted: In pure Fe, see

Deleted: 5

Deleted: our

Deleted: .

Deleted: the

Deleted: There

Deleted: to be a large effect of foil orientation for Fe^+ irradiations, with very 1

Deleted: a

Deleted: 100keV

Deleted: at RT

Deleted: Also shown on this plot are the earlier results of Kirk *et al* [14] which were obtained in {110} foils.

Deleted: 5

Deleted:

Deleted: pure

Deleted: (i.e. the defect yield was quite high, at about 0.04),

Deleted: Note also that there

Deleted: Argonne

Formatted: Font: Italic

Deleted: the

Deleted: at Oxford

Formatted: Font: Italic

Deleted: the

Deleted: 6

density by about a factor of two, or more. This plot also shows the effect of different irradiation temperatures for Xe⁺ irradiation in Fe11%Cr. Loop number densities at the same dose are lower at 300°C than at RT.

Deleted: consistently

3.2 Loop size distributions

Figure 5 shows image size distributions of visible loops in an Fe11%Cr foil irradiated with 100 keV Fe⁺ ions at RT, based on measurements of 200-300 loops at the higher doses, but only 21 loops at the lowest dose where the loop density is very low and so where statistics are poor. Note that all loops with image sizes < 2nm were put into the 1-2 nm bin – there is no 0-1 nm bin, since loops of such small size are unlikely to be seen. The mean image sizes are shown for each distribution together with the standard deviations of the measurements. There is no trend for a change in the image size distributions or mean image sizes with dose up to a dose of 3×10^{17} ions m⁻². Image sizes are not necessarily good indicators of the true sizes of individual loops of this size, but the mean image size is a good measure of the true mean loop size [26]. This result therefore suggests that loops do not grow after they have formed at these doses.

Deleted: 3.2.

Deleted: ¶

Formatted: Bullets and Numbering

Deleted: 7

Deleted: the

Deleted: self-ions

Formatted: Superscript

Deleted: room temperature

Deleted: the specimen shown in Fig. 2

Deleted: 0

Deleted: obvious

Deleted: image size distributions are reasonably good approximations to the true loop size distributions and

Deleted: 31

Deleted: 8

Deleted: pure

Deleted: (the Hawthorne alloy)

Deleted:

Figure 6 shows further size distributions for Fe11%Cr and polycrystalline 5N Fe irradiated under different conditions. The image sizes of loops produced by Xe⁺ irradiation have a wider distribution and larger mean size than those produced in the same material by Fe⁺ irradiation. Similarly the loops in Fe-11%Cr have a wider distribution and a larger mean size than those produced in pure Fe under the same irradiation conditions. The data at 300°C are more sparse because of the difficulty of maintaining a high foil quality through the course of the experiment. However for Fe-11%Cr irradiated with Xe⁺ ions there is not much difference in loop sizes between irradiation at RT and 300°C.

Loop size distributions were also measured for UHP Fe irradiated with 150 keV Fe⁺ ions at 300°C over a dose range 10^{17} - 2×10^{19} ions m⁻², both in *in-situ* and *ex-situ* experiments. At doses $\leq 10^{18}$ m⁻² the size distributions were narrow and peaked at about 2-3 nm, looking similar to the distributions shown in Figures 5 and 6. At higher doses the distributions broadened as more complex damage structures evolved in thicker areas of foil. These size distributions will be presented and discussed in Part 2.

Deleted: 7

Deleted: 3

Formatted: Font color: Auto

Deleted: 8

Deleted: 4

Formatted: Font color: Auto

Deleted: 3.3.

Formatted: Bullets and Numbering

Deleted: ¶

Formatted: Font: Times New

Deleted: difficult

Formatted: Font: Times New

Deleted: in these ferritic materials

Deleted: It was often impossible to tilt s

Formatted: Font: Times New

Formatted: Font: Times New

3.3 Loop morphologies

It was usually not possible to carry out complete diffraction contrast experiments because of the difficulty in tilting ferromagnetic specimens. Specimens could usually not be tilted by more than about 10-15° before it became impossible to correct astigmatism. Only in a few cases was it possible to characterize completely all the loops present (for an example see Part 2). Nevertheless several partial contrast experiments successfully distinguished loops with $\mathbf{b} = \frac{1}{2}\langle 111 \rangle$ from those with $\mathbf{b} = \langle 100 \rangle$.

Those of our specimens which were most favourably oriented for Burgers vector determinations were (001) single crystals of Fe, Fe-9%Cr and Fe-18%Cr. Small dislocation loops are expected to be invisible or to show very weak-contrast under weak-beam or kinematical diffraction conditions when $\mathbf{g} \cdot \mathbf{b} = 0$. Table 1 shows that a series of four images taken in the reflections available at a foil orientation $\mathbf{n} = [001]$ are sufficient for a fairly complete characterization of loop Burgers vectors. Only loops with $\mathbf{b} = [001]$ would not be seen at all. Just two images obtained in $\mathbf{g} = 200$ and $\mathbf{g} = 020$ are sufficient to distinguish between loops of type $\langle 100 \rangle$ and loops of type $\frac{1}{2}\langle 111 \rangle$.

Deleted: Also some variants of $\frac{1}{2}\langle 111 \rangle$ loops would not be distinguished. Even

Figure 7 shows such a contrast experiment in Fe9%Cr irradiated with 30 keV Ga⁺ ions in the FIB. The same area is shown imaged in three reflections, and some loops are ringed for easier identification. Both $\frac{1}{2}\langle 111 \rangle$ and $\langle 100 \rangle$ loops are present (see caption). Overall, of 102 loops in this area, 39 had Burgers vectors of type $\frac{1}{2}\langle 111 \rangle$ and 48 had Burgers vectors of type $\langle 100 \rangle$ whilst the Burgers vectors of 15 loops could not be assigned.

The results of two further successful experiments in 5N Fe and in Fe18%Cr are shown in Table 2. These both relate to *in-situ* room-temperature irradiations with 100 keV Fe⁺ ions. Also shown are the results of an analysis of loops in UHP Fe irradiated with 150 keV Fe⁺ ions at 300°C to a dose of 10^{18} ions m⁻² in a grain with orientation close to (011). A similar result was found in a specimen irradiated to 2×10^{18} ions m⁻².

Clearly there are insufficient data to be sure of trends. However in all cases $\langle 100 \rangle$ loops are in a majority. In Fe, $\langle 100 \rangle$ loops predominate. However, we also have to consider the possibility that $\frac{1}{2}\langle 111 \rangle$ loops are lost preferentially by glide to the surface. This is considered further in the discussion §4.2. The *in-situ* dynamical observations reported in §3.6 below, where loop loss to the surface was seen directly, throw further light on these observations.

3.4 Loop nature

It was not possible to determine the vacancy or interstitial nature of very small clusters in our *in-situ* experiments. The only reliable method for determining directly the nature of loops of size < 10 nm is the black-white (B-W) contrast technique. Loops lying close to the foil surface, within the so-called layer structure, may show B-W contrast under two-beam dynamical imaging conditions. If both the sense of the black-white vector **I** relative to the diffraction vector **g** and the depth of the loop in the layer structure are determined, its nature can be found (see reference [25] for a full discussion). Most loops produced by 100-150 keV ions however did not show B-W contrast, and it was not possible to measure accurately the depth of those which did by stereo microscopy [27]. For this reason we devised the following experiment. Loops were introduced into FeCr foils by 30 keV Ga⁺ ion irradiation in a FIB to a dose of 10^{18} ions m⁻² at RT. A SRIM calculation [22] showed that in this case the damage peak lies at 6nm and almost all damage lies within about 10 nm of the surface. Loops are therefore likely to be formed in the first depth layer, which in Fe-Cr alloys extends from the surface to a depth of about $0.3 \xi_g \approx 9$ nm, where ξ_g is the extinction distance for a {110} reflection. Figure 8 shows a micrograph of loops in Fe-11%Cr imaged under two-beam dynamical conditions. Several loops show clear B-W contrast and all have $\mathbf{g} \cdot \mathbf{l} > 0$. If these loops are in the first layer as expected, they are of vacancy type.

3.5 Loop losses during ion irradiation

Loops, once formed, were sometimes lost from the foil during or subsequent to ion irradiation. This effect was investigated in two ways. The first was by an analysis of micrographs recorded after each dose increment, following the fate of individual loops from one micrograph to the next. Since the resolution of films is excellent, loops as small as ~1-2 nm could be followed. This is described in this section. The second approach was by analysis of video recordings, which has the capability of seeing loops with short lifetimes of seconds or less, albeit at lower resolution than film. Since such loops appear and are then lost within a single dose increment, they would not be seen at all in film micrographs. This is described in §3.6.2.

Deleted: 9

Deleted: $g = 200, g = 020$ and $g = 110$

Formatted: ... [5]

Deleted: The loop which is visible in all three micrographs (dashed circle at top left) has $\mathbf{b} = \frac{1}{2} [1 \bar{1} 1]$ or $\frac{1}{2} [111]$. Those visible only in $g = 200$ and $g = 020$ (solid circles towards the top) have $\mathbf{b} = \frac{1}{2} [1 \bar{1} 1]$ or $\frac{1}{2} [111]$. Those visible only in $g = 020$ and $g = 110$ (dotted circles) have $\mathbf{b} = [010]$. Similarly those visible only in $g = 200$ and $g = 110$ (solid circles towards bottom) have $\mathbf{b} = [100]$.

Deleted: pure ... (Hawthorne all) ... [6]

Formatted: Font: Italic

Deleted: ¶

Formatted: Indent: First line: 0 pt, Space Before: 12 pt

Formatted: Font: Bold

Deleted: s.

Deleted: ¶

Formatted: Indent: First line: 0 pt, Space Before: 12 pt

Formatted: Font: Bold

Deleted: s.

Deleted: ¶

Formatted: Font: Not Italic

Deleted: The

Deleted: directly

Deleted: is difficult to determine

Formatted: Space Before: 12 pt

Deleted: ¶

Deleted: 3.4 . Nature of loops

Deleted: ¶

Formatted: Font: Bold

Formatted: Font: Italic

Deleted: technique of choice to determine the ... is ... the ... black-white ... black-white

Deleted: One of the more reliable methods is the so-called black-white contrast technique. Loops lying close to the foil surface may show black-w ... [8]

Deleted: ~

Deleted: In our experiments loop ... [9]

Deleted: black-white [10]

Deleted: The direction of **g** is marked.

Deleted: Those loops which sh ... [11]

Formatted: Font: Italic

Formatted: Heading 2

Deleted: ¶

Deleted: It was noticed that ... [12]

Figure 9 shows the same area of an Fe8%Cr specimen irradiated with 100 keV Xe⁺ ions at RT to four successive doses in increments of 10¹⁶ ions m⁻². The foil normal was close to [111]. This area was not illuminated with electrons during ion irradiation. The loops present after the first dose increment are marked by circles in the left-hand micrograph. In subsequent micrographs these loops are also marked by full circles if they are still present. If a loop has been lost from one dose to the next, its former position is shown as a broken circle in the next micrograph. Similarly loops which first appear after doses of 2, 3 and 4 x 10¹⁶ ions m⁻² are also ringed, and again broken circles indicate the former position of lost loops. The table below the figures shows: (1) the total number of loops seen in a field of view larger than, but encompassing, the area seen in Figure 9; (2) the number of new loops which appeared in this area during the dose increment; and (3) the number of loops which were visible in the previous micrograph but which disappeared during the new dose increment.

Deleted: 11

Deleted: a

Deleted: of 10¹⁶ ions m⁻²

Deleted: 11

Some loops persisted throughout the whole irradiation sequence. Others were lost at some point during the experiment, with varying lifetimes. In this example the number of loops actually decreased between doses of 3 x 10¹⁶ ions m⁻² and 4 x 10¹⁶ ions m⁻² because more loops were lost than gained.

Deleted: ¶

It is clear that some

Deleted: are

Deleted: Note that in

A similar experiment was performed in Fe11%Cr irradiated with 100keV Xe⁺ ions. Sequences of micrographs were recorded and analyzed after a succession of dose increments in areas with electron illumination and without electron illumination during ion irradiation, respectively. Figure 10 shows the results of this experiment. The areal densities of loops were smaller in the area irradiated with electrons, but the fraction of loops lost was similar in the two cases.

Deleted: 12

Deleted: It is clear that the

Deleted: are

Deleted: is

Formatted: Heading 2

Deleted: ¶

3.6 Dynamic observations

(This section should be read in conjunction with viewing the relevant video files)

3.6.1 Loop hopping

The motion of individual loops was observed in all materials. The motion took the form of sudden, discrete jumps or hops from one position to another over distances of several nanometers or more. Hops took place both during ion irradiation and under 200kV electron illumination alone. A full analysis of this phenomenon awaits more systematic and directed experiments, but we can make the following mostly qualitative observations:

- Small loops in UHP Fe were very mobile. Under a combination of ion irradiation and electron illumination a majority of loops not in very thin areas of foil executed a one-dimensional to-and-fro motion at both 300°C and RT. This is seen in video 1² (UHP Fe, 300°C) and video 2 (UHP Fe, RT). The linear feature in video 1 is a dislocation line used as a marker.
- Video 1 shows a (111) foil of UHP Fe under irradiation with 150 keV Fe⁺ ions at 300°C. Most loops are executing one-dimensional hops. The direction in which a loop moves is parallel to one of the three <211> directions lying in the foil plane. This is consistent with the glide of loops on their glide cylinders. It is not possible in this case to deduce the Burgers vectors of the

Deleted: A striking feature of the s

Deleted: was their extreme mobility

Deleted: (and similar features in other videos) are

Deleted: s

Deleted: s

² In order to play these .mpg files with RealPlayer you may need to install a mpeg-2 video codec, which is widely available as a free download on the web.

moving loops, since all $\frac{1}{2}\langle 111 \rangle$ and $\langle 100 \rangle$ Burgers vectors except $\frac{1}{2}[111]$ project parallel to these directions.

- Video 2 shows a (110) foil of UHP Fe under irradiation with 150 keV Fe^+ ions at RT. Again several loops are executing one-dimensional hops. In this case the Burgers vectors of the moving loops can be deduced from their directions of vibration. In this video the operating diffraction vector is $\mathbf{g} = \bar{1}\bar{1}0$. Under this condition the only loop variants we would expect to see are $\mathbf{b} = \frac{1}{2}[\bar{1}11]$ and $\frac{1}{2}[\bar{1}\bar{1}1]$ and $\mathbf{b} = [100]$ or $[010]$. Other variants have $\mathbf{g}\cdot\mathbf{b} = 0$ and so are out of contrast. The Burgers vectors of loops with $\mathbf{b} = \frac{1}{2}[\bar{1}11]$ or $\frac{1}{2}[\bar{1}\bar{1}1]$ lie in the plane of the foil, whereas the Burgers vectors of loops with $\mathbf{b} = [100]$ or $[010]$ project in the $[\bar{1}\bar{1}0]$ direction. It is found that all mobile loops move parallel to $[\bar{1}11]$ or $[\bar{1}\bar{1}1]$ directions and so have $\mathbf{b} = \frac{1}{2}[\bar{1}11]$ or $\frac{1}{2}[\bar{1}\bar{1}1]$. No loops are observed to move parallel to $[\bar{1}\bar{1}0]$. Therefore all hopping loops are of $\frac{1}{2}\langle 111 \rangle$ type. Observations over longer times than shown in video 2 showed that a majority of loops in this field of view hopped but at a lower frequency than at 300°C. However, about one quarter of the loops did not move at all.

Deleted: (of the four $\frac{1}{2}\langle 111 \rangle$ variants)

Deleted: (of the $\langle 100 \rangle$ variants)

Deleted: The other two $\frac{1}{2}\langle 111 \rangle$ variants and the $[001]$

Deleted: all

Deleted: most

- In UHP Fe, loops were frequently seen to hop under electron illumination alone, although the number of hopping loops was smaller than when the ion-beam was also hitting the specimen (video 3). In observations at 300°C, about one third of loops hopped when the electron beam was fully focused (in video 3, a count shows that 31 loops hop of a total of 81). The electron flux under this condition is estimated to be about $4 \times 10^{24} \text{ m}^{-2} \text{ s}^{-1}$. At room temperature the fraction of hopping loops was much smaller, less than 10%.

Deleted: we estimate that

Deleted:

Deleted:

- The frequency and amplitude of the jumps in UHP Fe under electron irradiation alone at 300°C was determined from analyses of successive video frames, and the results for several loops are shown in Figure 11. Jump distances were measured from video frames to the nearest nanometre. Some loops jumped over 10nm in a single hop. Hops usually took place from one video frame to the next or over two video frames, implying a velocity in excess of 10^3 nm s^{-1} . Loops hopped between two or more discrete locations, some spending most of the time in just one of these locations (see Figure 11(a)) and some distributing their time in different locations more evenly (Figure 11(b)-(d)).

Deleted: 13

Deleted: nanometer

Deleted: jump

Deleted: Jumps

Deleted: 13

Deleted: 13

- Hopping could be partially suppressed by adjusting the electron illumination condition. When the beam was spread until the image was barely visible (so reducing the electron flux by about a factor of 10) the number of loops which hopped was fewer. Some loops still hopped but at a much lower frequency. Video 4 shows the same area as video 3, with the electron beam spread: now only 14 of 81 loops hop. Of those loops which do hop, the frequency is much reduced but the amplitude remains much the same. Figure 11(e) shows measurements on the same loop as Figure 11(a) but with the electron beam intensity reduced. This loop hopped just once in 15 s compared with 16 hops in the same time interval when the electron beam was focused. The amplitude of the hop (4 nm) was however the same as in several previous cases (Figure 11(a)).

Deleted: 13

Deleted: 13

Deleted: 15 secs,

Deleted: 13

- In Fe of lower purity loop hopping was still observed frequently under combined electron and ion irradiation and occasionally under electron irradiation alone (see video 5). Loop hopping was less common in FeCr alloys but was seen occasionally. A comparison of loop hopping in

Deleted: (see video 6)

Fe8%Cr and pure Fe under the same irradiation conditions is shown in video 6. In both 5N Fe and Fe8%Cr, a smaller proportion of loops were involved than in UHP Fe. There was no obvious difference in the frequency and amplitude of jumps for those loops which did hop under combined ion and electron illumination, although quantitative measurements have not been made. There were insufficient data to make quantitative measurements of hopping under electron illumination in materials or conditions other than UHP Fe at 300°C.

Deleted: In both cases

- In all cases, loops in very thin areas of foil moved much less; most were more or less static even under combined ion and electron irradiation.

3.6.2 Dynamic observations on loop losses during and after ion irradiation

The loss of loops during ion irradiation was investigated by frame-by-frame analysis of video sequences. Not all video sequences were suitable for such analyses, since the specimen quality had to be very high for the smallest loops to be seen. The results are shown in table 3. The upper part of the table shows measurements on UHP Fe and Fe8%Cr irradiated with 150 keV Fe⁺ ions. In each case the initial dose was either “low” (i.e. about 5×10^{17} ions m⁻²) or “high” (i.e. about 4×10^{18} ions m⁻²). The accumulation and loss of loops was then measured for dose increments of 500-1500 counts (where 800 counts is equivalent to 10^{17} ions m⁻²). The lower part of the table shows some similar but less systematic measurements for several other material and irradiation combinations. The data are not sufficient to extract trends with complete confidence because of the large number of experimental parameters. A particularly important parameter is the foil orientation, which was not well controlled in these experiments. We note in this context that the experiment on UHP Fe at RT was carried out in a (110) foil, and at this orientation the Burgers vectors of two of the four $\frac{1}{2}$ <111> loop variants lie in the plane of the foil. Loops with these Burgers vectors cannot escape the foil by glide. In the (112) orientation used for the UHP Fe experiment at 300°C, one of the four $\frac{1}{2}$ <111> loop variants has **b** in the plane of the foil. At the other orientations all four $\frac{1}{2}$ <111> variants can glide to the surface.

Deleted: equates

Deleted: [

Deleted:]

Deleted: [

Deleted:]

With this in mind, we can make the following observations about table 3.

- In all cases considerable loss of loops occurred during irradiation.
- The rate of production of new loops did not seem to depend heavily or systematically on the material although the data are rather sparse. The rate of production of new loops was higher for Xe⁺ ions than for Fe⁺ ions. In UHP Fe the numbers of new loops per dose increment is smaller at high dose, although this trend is not seen in Fe8%Cr.
- In UHP Fe fewer loops were lost at higher damage levels than at lower. Looking at the summary rows in table 3 and the columns for new loops and new loops lost, 57% of new loops were lost at low dose and 38% at high dose. This observation may reflect a reduced mobility of loops in more damaged material.
- A higher fraction of loops were lost from pure Fe than from FeCr alloys for equivalent irradiation conditions. The effect of Cr may be to reduce loop mobilities, and hence loss to the surface. This effect is seen for example in comparing the two sets of data for UHP Fe and

Deleted: does

Deleted: is

Deleted: appear to be lost

Deleted: are

Deleted: are

Fe8%Cr irradiated with 150 keV ions at RT, where a smaller fraction of loops was lost in the latter case despite this being an orientation where most loops can glide to the surface.

- Loop losses appeared to be greater at higher temperature for the same materials and equivalent irradiation conditions, although the effect is fairly small and complicated by differences in orientation.

In addition to dynamic observations during ion irradiation, we also made video recording after irradiation (see §3.6.1). These recordings (videos 3 and 4) showed that loops in pure Fe sometimes vibrated backwards and forwards with an amplitude of several tens of nanometres under electron illumination alone. Frequently one of these vibrating loops was seen to be lost from the foil. We examine below (in §4.4) the possibility that the lower loop density in electron-irradiated regions is a result of loops escaping by electron beam assisted migration.

3.6.3 Time evolution of loop contrast

Frame-by-frame analysis showed that individual loops did not always appear more or less instantaneously, from one frame to the next. Instead the contrast of many loops built over several (3-5) frames, corresponding to a time interval typically of about 0.1 ~ 0.2 seconds. This observation was made for loops produced by both Fe⁺ and Xe⁺ ions and in both pure Fe and FeCr alloys, and at both RT and 300°C. There was no correlation between the final image size of the loop and the time taken for its contrast to saturate. The measurements which have been made to date are summarized in table 4.

Figure 12(a) shows an example of the appearance over several frames of a loop in Fe produced in an irradiation with 100 keV Xe⁺ ions at RT. Figure 12(b) shows measurements of the maximum image intensity of the loop for each frame. Figure 12(c) shows another example in the same specimen, where again the image intensity initially increased over about five frames. The contrast then remained constant, until after about a further 30 frames (~1 s – see the top scale) the loop suddenly disappeared. Figure 12(d) shows image intensities in successive frames of a loop in Fe8%Cr irradiated with 150 keV Fe⁺ ions at RT. This loop appeared within a single frame. These results are discussed in § 4.1.

§4 Discussion

The experiments described in §3 and especially the dynamic experiments described in §3.6 give interesting new insight into damage evolution in ferritic alloys under heavy ion irradiation. This is now examined.

4.1 The mechanism of loop formation

We have found that some loops in Fe11%Cr produced by *ex-situ* 30 keV Ga⁺ irradiation to a similar dose as our *in-situ* experiments are of vacancy nature, provided that they lay in the first depth layer, within about 0.3ξ_c of the ion-entry surface. It is difficult to be certain that this was the case, since the depths of individual loops were not measured directly. Accurate measurement of loop depths by stereo methods is difficult or even impossible (see ref [27]) and was not attempted. Although the SRIM calculations indicate that all damage was produced initially in the first depth layer, it could be argued that mobile loops could penetrate deep into the foil. Two facts however point to the probability that the loops analyzed were in the first depth layer. First, all showed strong B-W contrast. Simulations [26] show that B-W contrast is considerably stronger for first-layer loops than for loops in other layers. Second, all loops showing strong B-W contrast had g.l > 0, which suggests they were all in the same

Deleted: is

Deleted: ¶

Formatted: Indent: First line: 0 pt

Formatted: Heading 2

Deleted: ¶

Deleted: frames

Deleted: There are insufficient data to be sure of trends with composition or irradiation temperature.

Deleted: However, with the exception of Fe11%Cr irradiated with 100 keV Xe⁺ ions at RT, there does seem to be a systematic difference between loops produced by Xe⁺ ions and those produced by Fe⁺ ions. In the former case the contrast built up typically over 3-5 frames, and there were no examples of a sudden appearance from one frame to the next. In contrast, for Fe⁺ ions the timescale was shorter, typically 1-3 frames. There were several exam[... [13]

Deleted: 14

Deleted: 14

Deleted: 14

Deleted: 14

Formatted: Heading 3

Deleted: §

Deleted: ¶ [... [14]

Formatted: Heading 3

Deleted: ¶

Deleted: those

Formatted: Font: Italic

Formatted: Font: Italic

Deleted: which show strong bl[...] [15]

Deleted: most probably

Deleted: .

Deleted: This conclusion was [...] [16]

Formatted: Subscript

Deleted: , as suggested by SRI[...] [17]

Deleted: as

Deleted: , and is indeed

Deleted: to do

Deleted: I

Deleted: However only near-st[...] [18]

Deleted: , and the contrast is strongest

Deleted: .

Deleted: Further indirect evide[...] [19]

Deleted: all

layer and it unlikely that this layer would be other than the first. It does seem likely therefore that a proportion of the loops we see are of vacancy nature.

Deleted: .

This experiment does *not* show however that all of the loops in our experiments were of vacancy nature. Smaller loops not showing B-W contrast were also present and about these we can say nothing. In addition, it is probable that some loops were lost by glide to the surface. In the relatively thin (111) foil of the B-W experiment, most if not all of the mobile loops may have been lost in this way. The loops lost may predominantly have been of $\frac{1}{2}\langle 111 \rangle$ type, see §4.2. We have not yet analyzed loops in other alloys, nor have we been able to analyze loops produced by Fe^+ or Xe^+ ions.

Formatted: Font: Italic

Formatted: Indent: First line: 36 pt

Deleted: It should be noted that only larger near-surface loops have been analyzed

Deleted: Note however that s

Deleted: black-white

Deleted: . Smaller

Deleted: loops, or those located deeper in the foil, often do not show good black-white contrast,

Deleted: .

Deleted:

Deleted: It does

Deleted: however

Deleted: seem likely however that a proportion of the loops we see are of vacancy nature.

Deleted: We note that

Deleted: to higher doses

Deleted:

Deleted: 4

Deleted: 7

Deleted: 8

MD simulations of cascades in Fe and other materials suggest that direct clustering of interstitials as well as vacancies occurs within cascades e.g.[4, 12]. The clusters seen in these simulations are usually very small, probably sub-microscopic, and are likely to be highly mobile even at RT and so easily lost at surfaces [13]. It is nevertheless plausible that some of the loops we see are interstitial in nature, especially perhaps those located deeper in the foil. Further experiments, which we report in Part 2 throw further light on the loop nature, and suggest that interstitial clusters are present, at least at high doses.

Whatever the nature of the loops, our results suggest they form initially in some kind of cascade process. Evidence for this includes: (1) there is no dependence of the loop areal density on foil thickness at these doses (Figure 2), and (2) loops once formed do not increase in size at these doses (Figures 5 and 6). However the process does not generally seem to be athermal cascade collapse, which is believed to occur in metals such as Cu. In our experiments the defect yields, especially for Fe^+ irradiations, are very low, and by the time loops are seen several cascades must have overlapped spatially.

That loops do not form until cascade overlap occurs was also shown in one experiment which was carried out at high energy in an attempt to place loops more uniformly through the thickness of the foil. In this experiment, an Fe11%Cr foil was irradiated with 500 keV Fe^+ ions at RT to a maximum dose of 3.8×10^{18} ions m^{-2} . This results in an average damage level of about 1.8 dpa throughout the thickness of the foil according to a SRIM calculation. No loops were observed, even though loops were visible in this alloy at this dpa level in irradiations with 100 keV Fe^+ ions. Cascades produced by 500 keV ions break up into many small sub-cascades distributed over a large volume, and cascade overlap is still small at the highest dose in this experiment.

Deleted: .

Deleted: dose

Deleted: when irradiated

Further evidence pointing to the possible importance of pre-existing cascade debris is provided by the observation that loop number densities are reduced in irradiations at 300°C compared with RT for comparable irradiation conditions. This trend is best seen in the Xe^+ data for Fe11%Cr presented in Figure 4. At RT vacancies are immobile, and as the irradiation proceeds it would be expected that vacancy debris would accumulate with dose. However, at 300°C vacancies are mobile, so that partial annealing of the vacancy component of damage may occur. The background of cascade debris would build-up more slowly in this case and its morphology might be different. This would help explain a lower yield at the higher temperature.

Further insight into the process by which loops are formed is provided by our observations on the time evolution of the contrast of loops.

The appearance of loops over several video frames was something of a surprise and the possibility that this is an artifact should first be examined. The video frame repeat time is $1/29^{\text{th}}$ second, but frames are interlaced, and so changes which occur over one or two consecutive frames cannot be analyzed. Loop loss was often observed to occur within one or two frames, and so falls in this category. Many loops produced by Fe^+ ions also appeared over just 1-2 frames (see Table 4 and Figure 12(d)). We note however that in Figures 12(a) and (b) the image intensity increased over five consecutive frames before reaching a constant value. Image intensity increases over time scales from 3-5 frames were seen commonly (table 4). Note that the background intensity remained constant, and so this effect is unlikely to be an artifact due to intensity rescaling or the frame-grabbing software. Foil bending was also unlikely to be a problem since the appearance of the background did not change (Figure 12(a)). We conclude therefore that the effect is likely to be real.

The displacement phase of the cascade lasts only picoseconds, and cascade collapse has usually been regarded to occur on a similar (somewhat longer) timescale, within the lifetime of the thermal spike, $\sim 10^{-11}$ s, see e.g. [28]. As discussed in §1, cascade collapse has been observed in irradiations at low temperature (30K) where no thermal diffusion can occur, confirming that the process is at least partially athermal (e.g [9]). However, here we are unlikely to be dealing with cascade collapse as it is usually envisaged, especially in the case of Fe^+ irradiations. As discussed above, loops are likely to be produced in regions which contain debris from previous cascades. Loop formation is then considered to be triggered by the impact of a new cascade in a sea of dispersed sub-microscopic point-defect clusters. In such circumstances it is plausible that loop growth continues by diffusion of vacancies from the cascade periphery long after the thermal spike has subsided. Evidence of the role of thermal diffusion in loop formation under cascade-producing irradiation is provided by several of the low-temperature experiments alluded to in §1. For example, in Fe irradiated in-situ with Fe^+ ions at 30K, new loops appeared as the specimen warmed to room temperature, and existing loops grew [9]).

Recent Monte Carlo simulations on the long-term evolution of post-cascade radiation damage in iron at 500K by Hudson *et al* [29] suggest that vacancy clustering does occur on timescales consistent with our observations, even within isolated cascades. These authors found that the concentration of single vacancies dropped abruptly at a characteristic timescale of about 10^{-1} s (see their Figures 2, 3, and 5). This is just the time $L^2/2D_v$, for vacancies to diffuse a distance L equal to the spatial extent of a cascade. There is a possible trend in the results of table 4 for the image contrast to saturate over longer time scales in the case of loops produced by Xe^+ ions than for loops produced by Fe^+ ions, although the statistics are poor. Loops produced by Xe^+ ions are on average larger than those produced by Fe^+ ions, and so a plausible explanation for this observation is simply that larger loops take longer to reach their final size. However, no correlation was found between the time taken for the contrast to saturate and the final image size of the loop. We note however that the image sizes of individual loops depend strongly on the loop depth and foil thickness, and might be quite different from the actual loop size [26]. Further work is required on this phenomenon.

We conclude that our observations are consistent with loops first forming at cascade overlap doses by the mechanism suggested by Robertson *et al* [9], as described in §1. Some loops then grow to their final sizes in timescales of the order of 0.1-0.2 s by local vacancy agglomeration.

4.2 Effects of Cr on damage development

Deleted: 14

Deleted: 14

Deleted: in the case of Xe^+ irradiation

Deleted: 14

Deleted: 33

Deleted: i overlap doses,

Deleted: 34

Deleted: of a second

Formatted: Font color: Auto

Formatted: Font color: Auto

Formatted: Font color: Auto

Formatted: Font color: Auto

Formatted: Superscript

Formatted: Superscript

Deleted: ¶

Formatted: Font color: Auto

Deleted: delete¶

This model also provides a possible qualitative explanation of why clustering often occurs over longer time scales in the case of cascades produced by Xe^+ ions than in cascades produced by Fe^+ ions. Cascades produced by Xe^+ ions are expected to be compact with relatively little sub-cascade formation. The diffusion distance L in this case would be the radius of the total cascade. In the case of Fe^+ irradiation, cascades on average are more diffuse and break up into sub-cascades. We then envisage loop formation to occur when a new sub-cascade impinges on a region of high vacancy concentration. The mechanism of loop formation is essentially the same as for Xe^+ ions – first the formation of a loop nucleus on a very short time scale, followed by accretion of local vacancies by diffusion. However the characteristic diffusion distance L is now the radius of the sub-cascade, which on average will be smaller, leading to a shorter diffusion time. In this case loop growth due to diffusion is likely to be more limited, leading to smaller loop sizes in agreement with our observations (Fig. 8). ¶

¶ We speculate that the exceptional case of Fe11%Cr irradiated with 100 keV Xe^+ ions at room temperature, when loops did not appear over more than 3 time frames, may be related to the low dose at [... [20]

Formatted: Font color: Blue

Deleted: above

Deleted: These

Deleted: vacancy

Deleted: diffusion

4.2.1 Effect of Cr on loop morphologies

Dislocation loops both with $\frac{1}{2}\langle 111 \rangle$ and $\langle 100 \rangle$ Burgers vectors were present both in pure Fe and in Fe 8% and 11%Cr alloys. The fraction of $\frac{1}{2}\langle 111 \rangle$ loops in the (001) FeCr alloys was of the order of 40%. The loop Burgers vectors in pure Fe however were predominantly of $\langle 100 \rangle$ type. The presence of a substantial fraction of $\frac{1}{2}\langle 111 \rangle$ loops in Fe-Cr alloys is consistent with work on neutron-irradiated materials [30-33]. Similarly, mostly $\langle 100 \rangle$ loops have been found in neutron-irradiated pure Fe. However, the loops in all these cases were probably interstitial in nature [30-34], whilst we may be dealing largely with vacancy loops or with a mixed vacancy/interstitial loop population.

At least two factors may contribute to our observations. First, our dynamic experiments have shown that more loops are lost during irradiation of Fe than of FeCr alloys. Several mechanisms may cause such loss. Loops may be annihilated by the impact of a cascade; they may convert to a morphology such as a small void, which is invisible in the microscope; or they may be lost by glide to the surface. The first two mechanisms would not be expected to depend strongly on the alloy composition. The observation of vibrating loops during and after ion irradiation suggest that glide to the surface is the most probable loss mechanism, and indeed vibrating loops were occasionally seen to be lost under electron irradiation alone. The low loop yields in (111) Fe foils (Figure 3) and the smaller average sizes of loops in pure Fe compared with Fe11%Cr (Figure 6) are also consistent with loss of larger loops to the surface. Daulton *et al* [21] carried out frame-by-frame analyses of loop losses in elevated-temperature ion irradiations of copper, and also concluded that glide to the surface was the most likely loop loss mechanism.

Loop loss to the surface is thought to occur under the influence of surface image forces [35]. Gilbert *et al* [13] estimate that $\frac{1}{2}\langle 111 \rangle$ loops in pure Fe lying within 5 nm of a (111) surface may be lost within about 100ps at 500K. This timescale is beyond the reach of our experiments. It is therefore possible that our dynamic experiments on loop loss described in §3.6.2 misses a population of loops with very short lifetimes, although in real materials loops may be less mobile due to trapping by impurities and Cr atoms and so timescales may be longer. Loop migration may also be stimulated by the ion and electron beams as discussed in §4.4 below.

The contrast experiments were carried out in single crystals of orientation (001). In an (001) foil, loops with $\mathbf{b} = [100]$ and $[010]$ would be retained in the foil, since \mathbf{b} has no component towards the surface. The glide cylinders of all $\frac{1}{2}\langle 111 \rangle$ variants however intersect the surface, making an angle of 54.7° with the foil normal \mathbf{n} , and so a proportion of these loops (probably larger loops lying shallow in the foil) will be lost. The difference in the fractions of loops of the two types in different materials may then be explained if $\frac{1}{2}\langle 111 \rangle$ loops are more easily lost to the surface in Fe than in FeCr alloys. Both our dynamic experiments and our number density measurements suggest that this is the case, as discussed below.

Surface effects may also influence the morphology of loops – those with Burgers vectors with large components towards the surface may be produced more readily [36]. This would not however explain the different proportions of $\frac{1}{2}\langle 111 \rangle$ and $\langle 100 \rangle$ loops in Fe and FeCr alloys.

A second possibility to explain the different proportions of $\frac{1}{2}\langle 111 \rangle$ and $\langle 100 \rangle$ loops in different materials is that $\langle 100 \rangle$ loops are energetically more favoured in Fe than in FeCr alloys. There does not seem to have been any theoretical work on this. In pure Fe, Gilbert *et al* [13] find in atomistic

Deleted: L

Deleted: ¶

Deleted: both

Deleted: 17-20

Formatted: Font color: Auto

Deleted: Note h

Deleted: that

Deleted: 17, 18, 20, 35

Deleted: are probably

Deleted: :

Deleted: :

Deleted: loops

Deleted: L

Deleted: is also consistent with loss of loops by glide to the surface.

Deleted: 26

Deleted: 36

Deleted: g,b

Deleted: [

Deleted:]

Deleted: [

Deleted:]

Deleted: those most shallow in the foil

Deleted: We note that surface

simulations that very small circular $\langle 100 \rangle$ loops are more stable than $\frac{1}{2}\langle 111 \rangle$ loops and the two loop types then have comparable energies up to sizes of about 3 nm. Rectilinear $\langle 100 \rangle$ loops have even lower energy. Our observation that there is a preponderance of $\langle 100 \rangle$ loops in pure Fe is consistent with this.

4.2.2 Effect of Cr on loop number densities

Our dynamic experiments have shown that loop density measurements are strongly affected by loop loss during and sometimes after irradiation. We now examine if differential loss of loops to the surface account for the apparent differences in yields between pure Fe and FeCr alloys seen in Figures 3 and 4. Several of our observations suggest that this may be the case.

- Our dynamic experiments reported in § 3.6.2 suggested that the number of loops produced in FeCr alloys and pure Fe were similar, but more loops were lost to the surface during irradiation in the latter case.
- Loop hopping is much more prevalent in UHP Fe than in FeCr alloys, and vibrating loops were occasionally seen to leave the foil.
- Measured loop densities were found to depend strongly on the foil orientation in pure Fe, but not in Fe11%Cr. In pure Fe, loop number densities were higher in foils of orientation (110) than (111) or (001) for equivalent irradiation conditions. In a (110) foil, two $\langle 111 \rangle$ directions and [001] lie in the foil plane and loops with Burgers vectors parallel to these directions are not able to glide to the surface. In (111) and (100) foils a high proportion of loops, may have been lost. In the Fe11%Cr alloy however, the loop number densities after FIB irradiation were not dependent on foil orientation.

These observations suggest that Cr acts to reduce loop mobility, leading to less loss of loops to the surface in FeCr alloys compared with pure Fe. Terentiev *et al* [36] have shown that a reduction in mobility of self-interstitial clusters in FeCr alloys relative to pure Fe is to be expected. Its origin is a long-range, attractive interaction between Cr atoms and crowdions. Simulations have not yet been made for the interaction between Cr atoms and vacancy clusters, but a similar effect is plausible.

4.3 Other trends in loop density measurements

Notwithstanding the conclusion of the previous section that differential loop losses strongly affect loop density measurements, and the limited number of our experiments, it is still possible to discern some trends:

- The slopes of the log-log plots of loop density versus dose varied with material and irradiation conditions. Loop number densities N increased with dose ϕ at a rate $N = \phi^n$ with $n \approx 0.7 - \sim 2$ (see Figures 3 and 4). A slope $n = 1$ implies that the loop production rate is constant with dose, sometimes regarded as evidence that loops are produced within individual cascades. Kirk *et al* [37] attributed a slope $n < 1$ to loop coalescence and loop loss by cascade-loop overlap, both of which become more likely with increasing dose. Our experiments, including direct dynamical observations, show evidence of such saturation behaviour (see § 3.6.2 and the associated videos and Figure 9). A slope greater than unity is expected if loops are produced predominantly by the cascade overlap mechanism [37]. A slope $n > 2$ can arise if loss of loops to the surface is more probable at lower doses than higher doses. This may be particularly significant in pure Fe, when

Deleted: L

Deleted: We have found that surviving loop number densities were higher in Fe-Cr alloys than in pure iron for equivalent irradiation conditions, with the largest increase for 11%Cr (Figure

Deleted: 5

Deleted: 3). However it is clear

Deleted: An obvious question presents itself: can

Deleted: ?

Deleted: the answer to this question is "yes":

Deleted: not dissimilar

Deleted: 100

Deleted: 111

Deleted: In the first orientation, used by Kirk *et al* [14], t

Deleted: a (110)

Deleted: In our experiments, grains of $\langle 110 \rangle$ orientation were generally not present, and so we were constrained to work with polycrystalline foils in grains with normals close to $\langle 111 \rangle$ or single crystal foils with normal [001].

Deleted: both of these orientations

Deleted: especially those with $b = \frac{1}{2}\langle 111 \rangle$,

Deleted: 37

Deleted: §

Deleted: In our experiments the

Formatted: Bulleted + Level: 1 + Aligned at: 18 pt + Tab after: 36 pt + Indent at: 36 pt

Deleted: loop

Deleted: curves

Deleted:

Deleted: in most materials

Deleted: 5

Deleted: 6

Deleted: 38

Deleted: saturation behaviour such as

Deleted: 11

Deleted: can arise

Deleted: due to

Deleted: loop 1

Deleted: es

Deleted: , which

mobile loops may easily be lost at low doses, but are more likely to be pinned in the foil by cascade debris at higher doses. This is consistent with our dynamical experiments reported in § 3.6.2 and is the likely explanation for the slope $n > 2$ for (111) Fe irradiated with 100 keV Fe⁺ ions seen in Figure 3.

- Loop densities increased with the mass of the bombarding ion. This is consistent with earlier work [6-8]. It has generally been argued that an increase in mass leads to more compact cascades with a larger propensity to collapse. In the case of Fe11%Cr and Fe8%Cr irradiated with 100 keV Xe⁺ ions at RT, loops were first seen at a dose of only 10^{16} ions m⁻², when cascade overlap is low. In Fe the threshold dose was somewhat higher (2×10^{16} ions m⁻²) for the same irradiation conditions. In these cases, some collapse of individual cascades may be taking place as in earlier experiments with ions more massive than Fe [8]. Calder *et al* [38] have recently investigated by MD the effect of mass of the primary knock-on atom on displacement cascade debris in Fe. These authors found, perhaps surprisingly, that on average fewer point-defects were produced with increasing PKA mass. However cluster sizes were larger for more massive PKAs, and there was a correlation between the production of large vacancy and interstitial clusters in the same cascade. They saw in their simulations the production of interstitial loops of $\frac{1}{2} \langle 111 \rangle$ type, and both vacancy and interstitial loops of $\langle 100 \rangle$ type within individual cascades created by molecular ions. The tendency for $\langle 100 \rangle$ loops to be produced increased with both PKA mass and energy. These simulations are in qualitative agreement with our observations.

- Loop number densities decreased with increasing irradiation temperature in Fe11%Cr (Figure 4). We have argued above that changes in the background vacancy debris may lead to lower loop production at 300°C than at RT. There was also evidence in the dynamic observations that more loop losses occurred at 300°C than RT.

4.4 Loop hopping and electron irradiation effects

Similar one-dimensional (1-D) back-and-forth motion of small clusters in Fe and several other materials under high-voltage electron irradiation has been reported previously by other authors [e.g. 39-42]. The most relevant study is that of Satoh *et al* [42], who carried out a systematic investigation of the effects of impurities on the 1-D migration of interstitial clusters produced in Fe by 1.25 MeV electron irradiation at RT. Loops were seen to jump in sudden discrete steps in a very similar manner to the present experiments (see, for example their figure 2 which should be compared with our figure 11). Jump distances were sometimes over 100 nm in very high purity Fe, but were generally less than 30 nm in less pure Fe. The jump rate was approximately proportional to the electron intensity. Satoh *et al* found that the distribution of jump distances in specimens of different purity was consistent with the assumption that in their specimens interstitial clusters are trapped by interactions with impurity atoms. They considered on the basis of a molecular dynamics model that detrapping occurred when impurity atoms were displaced by collisions with fast electrons. The loop is then able to migrate rapidly before becoming trapped by other impurities.

Loop hopping in Fe under ion-irradiation has not been reported previously. However, Abe *et al* [43] have reported loop hopping in copper and gold produced by *in-situ* ion irradiation at 573-823K. In their case, initially sessile clusters (Frank loops) transformed into glissile clusters (prismatic loops),

Deleted: . This is because loops

Deleted: may be particularly significant in pure Fe, and

Deleted:

Deleted: 5

Deleted: There is a trend for loop

Formatted: Bulleted + Level: 1 + Aligned at: 18 pt + Tab after: 36 pt + Indent at: 36 pt

Deleted: to

Deleted: 39

Deleted: There is a trend for loop

Formatted: Bulleted + Level: 1 + Aligned at: 18 pt + Tab after: 36 pt + Indent at: 36 pt

Deleted: to

Deleted: .

Deleted: A similar trend has been seen in previous experiments in other materials. In the *in-situ* experiments of Daulton *et al* [

Deleted: 26

Deleted: 21] in ion-irradiated Cu, a drop in defect yield at temperatures above 300°C was not thought to be due to loop loss during or following ion irradiation, but rather reflected a decrease in the probability of cascade collapse. In our experiments we consistently saw lower loop densities at 300°C than at RT for foils of the same orientation (Figures 5(a) and 6). There was however evidence in the dynamic observations that more loop losses occurred at 300°C than RT, which accounts for at least part of this observation.

Deleted: ¶

Deleted: fro

Formatted: Font: Italic

Deleted: The discrete hops executed by loops under ion and electron irradiation suggest that they jump from one local position of equilibrium to another in the elastic fields created by impurities or other defects.

Formatted: Font: Italic

Deleted: has been reported by Abe *et al* [40].

which then oscillated with an amplitude typically of about 5 nm and a frequency of 1s^{-1} or more and velocities ranging from 50 to $>10^3\text{ nm s}^{-1}$. In addition Abe *et al* reported the existence of very small clusters with lifetimes of the order of a few thirtieths of a second. It was not clear if these clusters were lost by glide to the surface or by thermal evaporation, but the former seems likely. Abe *et al* considered that these very small clusters were most likely of interstitial character, since their directions of motion were along expected crowdion directions.

Our observations are consistent with the general picture of Satoh *et al*. [42]. We also observe reduced loop hopping in lower purity 5N Fe compared with UHP Fe, suggesting that the energy barrier for loop hopping depends on the impurity concentration. Loop hopping was much less prevalent in FeCr alloys than in Fe, suggesting that in this case Cr further reduces loop mobility. In our case the situation is complicated by the likely presence of cascade-induced damage which may further inhibit loop motion. In addition, it is quite possible that both vacancy and interstitial loops are present, and both species may be hopping. Recent atomistic simulations by Gilbert *et al* [13] suggest that $\frac{1}{2}\langle 111 \rangle$ loops in Fe of both vacancy and interstitial nature have high diffusivities.

In an Fe foil of orientation (110) only loops with $\mathbf{b} = \frac{1}{2}\langle 111 \rangle$ were seen to vibrate. There are two possible reasons for this. First, loops with $\mathbf{b} = [100]$ or $[010]$ have glide cylinders inclined in the foil, and so may have been lost to the foil surface. Second, $\langle 100 \rangle$ loops may be less mobile than $\frac{1}{2}\langle 111 \rangle$ loops. About a quarter of the loops did not move under electron irradiation and it possible that these sessile loops had $\mathbf{b} = \langle 100 \rangle$, but this cannot be said with certainty. In Satoh *et al*'s electron irradiation experiment [42], loops with $\mathbf{b} = \frac{1}{2}\langle 111 \rangle$ were found to be much more mobile than $\langle 100 \rangle$ loops, and this was put down to their smaller elastic interaction with impurity atoms. In our experiments, very few loops in very thin regions of the foil moved. It is possible that in these regions all mobile loops were lost to the foil surfaces soon after their formation.

Both we and previous authors have found that hopping can occur under sub-threshold (200kV) electron irradiation alone. Both we and Satoh *et al* [42] found that in this case only a small proportion of the loops executed hops, whereas under irradiation with ions or 1.25 MeV electrons a majority of loops hopped. Satoh *et al* suggested that in the case of loops which hopped under sub-threshold electron irradiation, the trapping was caused by impurities with relatively weak binding. Detrapping can also occur thermally, but hopping is unlikely to be due to beam heating. Under electron irradiation alone with a focused beam the temperature rise of the specimen in our experiments was calculated to be just a few degrees.

The mechanism by which sub-threshold electron irradiation suppresses the defect yield is not yet clear. One possibility is that loop losses to the surface are higher in regions which are illuminated with electrons during ion irradiations. On the other hand, Figure 10 shows that a similar proportion of loops are lost in illuminated regions and in regions outside the beam, suggesting that electron irradiation may have a direct effect on loop formation. This is certainly plausible: for example, sub-threshold electron irradiation could free point-defects trapped by carbon atoms leading to greater recombination, or electron-assisted vacancy migration could affect the cascade debris.

§5 Summary and Conclusions

Deleted: Clearly o

Formatted: Font: Italic

Deleted: In our case we are probably dealing with small prismatic dislocation loops with Burgers vectors $\frac{1}{2}\langle 111 \rangle$ or $\langle 100 \rangle$ and of unknown nature.

Deleted: Q

Deleted: possibly

Deleted: [

Deleted:]

Deleted: explanations

Deleted:

Formatted: Font: Italic

Formatted: Font: Bold

Deleted: larger

Deleted: V

Formatted: Font: Italic

Deleted: almost all

Formatted: Font: Italic

Deleted: in such cases

Deleted: The discrete hops executed by loops under ion and electron irradiation suggest that they jump from one local position of equilibrium to another in the elastic fields created by other cascade-generated defects. Reduced loop hopping in lower purity Fe suggests that the presence of impurities increases the energy barrier for loop hopping. Loop hopping is much less prevalent in FeCr alloys, suggesting that in this case Cr further reduces loop mobility. ¶

¶ Hopping is clearly stimulated by both the ion and electron beams. Note that hopping is unlikely to be due to beam heating. Under electron irradiation alone with a focused beam the temperature rise of the specimen was calculated to be just a few degrees. A proper analysis of the mechanism has not yet been attempted. Loop hopping will be analysed in greater detail in a future publication.¶

Deleted: also

Deleted: 12

Deleted: Alternatively loop losses may be occurring by mechanisms other than loss to the surface, such as loop dissolution by cascade overlap, which would lead to the same trend.

1. The evolution of radiation damage under heavy-ion irradiation in thin foils of pure Fe of various purities and a range of FeCr alloys has been investigated. In this paper we have described damage development at doses up to 2×10^{18} ions m^{-2} (~ 1 dpa) in irradiations at RT and 300°C.
2. In all materials, small (2-4 nm) dislocation loops first appeared at doses between about 10^{16} and 10^{17} ions m^{-2} . At these doses strong spatial overlap of cascades occurs. Loops with both $\langle 100 \rangle$ and $\frac{1}{2} \langle 111 \rangle$ Burgers vectors were identified. There was some evidence that loops with $\mathbf{b} = \langle 100 \rangle$ predominated in pure Fe, whilst the two types of loop were present in comparable numbers in FeCr alloys. A possible reason for this is that $\frac{1}{2} \langle 111 \rangle$ loops in pure Fe, which we have found to be very mobile, are preferentially lost from the foil. *Ex-situ experiments suggested that at least some of the loops are vacancy in nature*
3. The number densities N of loops retained in the foil increased with dose ϕ according to $N = \phi^n$, with n ranging from about 0.7 to ~ 2 according to material and irradiation conditions. Low values of n are probably due to saturation effects, and high values due to loss of glissile loops to the surface. Loop number densities at a given dose: (i) were higher for Xe^+ irradiation than for Fe^+ irradiation of the same material at the same temperature; (ii) *were only weakly dependent on Cr content for equivalent irradiation conditions*; and (iii) *in Fe11%Cr* were lower for 300°C irradiations than for equivalent RT irradiations.
4. Loop size distributions in Fe11%Cr did not change with dose at doses below 2×10^{18} ions m^{-2} , implying that loops did not grow after they had formed and suggesting they were produced in some sort of cascade event. Average loop sizes were: (i) larger in Fe11%Cr than in equivalent irradiations of pure Fe; (ii) in Fe11%Cr were larger in irradiations with Xe^+ ions than in equivalent irradiations with Fe^+ ions, and (iii) in Fe11%Cr were larger in an irradiation at RT compared with an irradiation at 300°C.
5. The contrast of individual loops developed over several video frames, especially for Xe^+ irradiations. This is in accord with a model where loops nucleate within cascades or sub-cascades, and then grow to their full size by accumulating vacancies from the cascade peripheries by diffusion.
6. Several observations (see 7-9 below) suggest that the main effect of Cr is to pin loops and so reduce their mobilities.
7. In pure Fe, the loop number densities depended strongly on the foil orientation. They were lowest in (111) foils and highest in (110) foils. In Fe11%Cr, the loop number densities were independent of foil orientation in 30 keV Ga^+ ion irradiations.
8. Loss of loops by glide to the surface or other mechanisms was seen frequently, both during ion irradiation and after. The number of loops retained in the foil was strongly dependent on the foil orientation and material. In pure Fe loops were very mobile and frequently lost if the glide cylinder of the loop intersected the surface. More loops were retained in FeCr alloys than in pure Fe for the same irradiation conditions. These observations are explained if loops are less able to escape the foil by glide in FeCr alloys than in pure Fe. It is possible that this effect

Deleted: by both *ex-situ* TEM and *in-situ* experiments

Formatted: Font: Italic

Deleted: A

Deleted:

Deleted: increased with increasing

Deleted: of the material

1
2 alone explains why loop number densities are higher in FeCr alloys than in pure Fe for
3 comparable irradiation conditions.

Deleted: the same

- 4
5 9. Loop hopping in discrete jumps often of several nanometres occurred during ion irradiation and
6 could also be induced by the electron beam alone. Hopping was particularly pronounced in
7 ultra-pure (UHP) iron, but occurred much less frequently in FeCr alloys. Some hopping loops
8 certainly had $\frac{1}{2}$ $\langle 111 \rangle$ Burgers vectors. No cases were found in which $\langle 100 \rangle$ loops definitely
9 hopped.

Deleted: It

Deleted: was not always possible to determine the Burgers vectors of hopping loops. However, s

- 10
11 10. Loop number densities were lower in regions of the foil which were illuminated with electrons
12 during ion irradiation. This may be due to enhanced loss of loops by electron assisted migration,
13 or by an effect of the electron beam on loop formation.

Formatted: Font: 11 pt

Formatted: Font: 11 pt

Acknowledgements

The IVEM-Tandem Facility (within the Electron Microscopy Center at ANL) is supported by the US DOE Office of Science and operated under contract no. DE-AC02-06CH11357 by UChicago Argonne, LLC. We thank Dr. A. Liu and P Baldo of Argonne National Lab for their help in using this facility. Part of this work was funded by the UKAEA, Culham Science Centre. We thank Prof. J. Le Coze of the École de Mines de Saint Étienne for the provision of UHP iron. We are grateful to Dr. S. L. Dudarev, Dr C A English and M. Gilbert for helpful discussions.

Deleted: *Ex-situ* experiments on UHP Fe were supported by the European Commission in the framework of the PERFECT Project.

For Peer Review Only

References

1. D.S. Gelles, J.Nucl. Mater. **233-237 A**, 293 (1996).
2. R.L. Klueh and D.R. Harries, *High Chromium Ferritic and Martensitic Steels for Nuclear Applications*, American Society for Testing and Materials, West Conshohocken, PA, USA (2001).
3. K. Ehrlich, Fus. Eng. Des. **56-57** 71 (2001).
4. A.F. Calder and D.J. Bacon, J. Nucl. Mater. **207** 25(1993)
5. C A English and M L Jenkins J. Nucl.Materials , **96** 341 (1981).
6. C A English and M L Jenkins , Mater. Sci. For. **15-18** 1003 (1987).
7. M. L Jenkins, M. A Kirk and W.J Phythian, J Nucl. Mat., **205** 16 (1993)
8. M.L Jenkins, C.A English and B L Eyre, Phil. Mag., **38** 97 (1978).
9. I. M. Robertson, M.A. Kirk and Wayne E. King, Scripta Met. **18** 317 (1984).
10. B. L Eyre and R. Bullough, Phil.Mag. **11** 31 (1983)
11. A. Dunlop, B. M. Pande, K. Böning, P. Rosner and H. E. Schaefer, J. Nucl. Mat. **108 & 109** 83 (1982)
12. N. Soneda, S. Ishino and T. Diaz de la Rubia, Phil Mag. Lett. **81** 649 (2001)
13. M Gilbert , S. L. Dudarev, P. Derlet, and D. G. Pettifor submitted to Journal of Physics: Condensed Matter (2008)
14. M. A. Kirk, I. M. Robertson, W. E. King, W. E. Ryan and A. Philippedes, Material Research Society Proceedings, vol. **41**, 315 (1985).
15. H.Fukushima, K Shimomura and H Yoshida, J Nucl. Mat., **141-143** 16 (1986)
16. H Fukushima, M L Jenkins and M A Kirk, Phil Mag **A75** 1567 (1997).
17. F. A. Garner, M. B.Toloczko and B. H. Sencer, J. Nucl. Mat. **273**, 123 (2000).
18. A Nicol, M.L Jenkins and M.A. Kirk, Proceedings of MRS Fall meeting, Symposium R: Microstructural processes in irradiated metals, Mat. Res. Soc. Symp. Proc. **650** R1.3 (2001).

Deleted: ¶

Deleted: <#>D.S Gelles, J Nucl. Mat., **108 & 109** 515 (1982).¶

¶<#>S.I Parollo, A.M Dvoriashin, A.N Vorobyev and Yu. V Konobeev, J Nucl. Mat., 256, 247 (1998) ¶

¶<#>Yu.V. Konobeev, A.M. Dvoriashin, S.I. Porollo and F.A. Garner, J. Nucl. Mat, **355** 124 (2006)¶

¶<#>M. Matijasevic and A. Almazouzi (private communication, 2007).¶

¶<#>R. Schäublin and M. Victoria, Mat. Res. Soc. Symp. Proc. Vol. **650**, R1.8.1 (2001).¶

Formatted: Bullets and Numbering

Formatted: Bullets and Numbering

19. Z. Yao, S.Xu, M. L. Jenkins and M.A.Kirk, [Journal of Electron Microscopy; doi:10.1093/jmicro/dfn004](#) (2008). **Formatted:** Bullets and Numbering
Deleted: submitted to J. Electron Microscopy
20. C.W.Allen, L.L.Funk and E.A. Ryan, *Mat. Res. Soc. Symp. Proc. Vol 396* 641 (1996). **Deleted:** 2007
21. T.L.Daulton, M.A.Kirk and L. Rehn, *Phil. Mag.* **A80** 809 (2000). **Deleted:**
22. J.F Ziegler and J.P Biersack, *The stopping and range of ions in matter, SRIM-2003*, ©1998, 1999 by IB77M co. **Formatted:** Bullets and Numbering
23. P. G. Lucasson and R. M. Walker, *Phys. Rev.* **127**, 485 (1962) **Formatted:** Bullets and Numbering
24. P. Jung, *Phys. Rev. B* **23**, 664 (1981) **Formatted:** Bullets and Numbering
25. M L Jenkins and M A Kirk, *Characterisation of Radiation Damage by Transmission Electron Microscopy*, Institute of Physics Series in Microscopy in Materials Science (Series Editors, B Cantor and M J Goringe) ISBN 0 7503 0748 X (hbk) (2001) **Formatted:** Bullets and Numbering
26. Z. Zhou, M L Jenkins, S L Dudarev, A P Sutton and M A Kirk, *Phil. Mag.* **86**, 4851, (2006). **Formatted:** Bullets and Numbering
Deleted:
27. H Fukushima, M L Jenkins and M A Kirk, *Phil.Mag.* **A75** 1583 (1997) **Formatted:** Bullets and Numbering
28. V.I Protasov and V.G Chudinov, *Radiation Effects*, **66** 1 (1982) **Formatted:** Bullets and Numbering
29. T. S Hudson, S.L Dudarev, M.J Caturla and A.P Sutton, *Phil. Mag.* **85** 661 (2005) **Formatted:** Bullets and Numbering
30. D.S Gelles, *J Nucl. Mat.*, **108 & 109** 515 (1982). **Formatted:** Indent: Left: 18 pt
Formatted: Bullets and Numbering
31. S.I Parollo, A.M Dvoriashin, A.N Vorobyev and Yu. V Konobeev, *J Nucl. Mat.*, **256**, 247 (1998) **Formatted:** Bullets and Numbering
Formatted: Indent: Left: 18 pt
32. M. Matijasevic and A. Almazouzi (private communication, 2007). **Formatted:** Bullets and Numbering
33. R. Schäublin and M. Victoria, *Mat. Res. Soc. Symp. Proc. Vol. 650*, R1.8.1 (2001). **Formatted:** Numbered + Level: 1 + Numbering Style: 1, 2, 3, ... + Start at: 1 + Alignment: Left + Aligned at: 18 pt + Tab after: 36 pt + Indent at: 36 pt, Widow/Orphan control
34. B.C Masters, *Phil. Mag.*, **11** 881 (1965) **Formatted:** Font: Times New Roman, English (U.S.), Condensed by 0.15 pt
35. W. Jäger and M. Wilkens, *Phys. Stat. Sol.* **A32**,89 (1975) **Formatted:** Bullets and Numbering
36. D. Terentyev, L. Malerba and A. V. Barashev, *Phil Mag. Lett.* **85**, 587 (2005). **Formatted:** Bullets and Numbering
37. M.A. Kirk, I. M. Robertson, M. L.Jenkins, C.A.English, T.J.Black and J.S.Vetrano, *J. Nucl. Mat.* **149**, 21 (1987) **Formatted:** Bullets and Numbering
Formatted: Bullets and Numbering
38. A. F. Calder, D. J. Bacon, A. V. Barashev and Yu. N. Osetsky, *Phil. Mag. Lett.* **88**, 43(2008) **Formatted:** Bullets and Numbering

39. M. Kiritani, J. Nucl. Mat. **251**, 237 (1997)

Formatted: Bullets and Numbering

40. T. Hayashi , K.Fukumoto and H. Matsui, J. Nucl. Mat. **307-311**, 993 (2002)

Formatted: Font: Bold

41. Y. Matsukawa and S. J. Zinkle, Science 318, 959 (2007)

Formatted: Font: Bold

Formatted: Bullets and Numbering

42. Y. Satoh, H. Matsui and T. Hamaoka, Phys. Rev. B77, 94135 (2008)

Formatted: Bullets and Numbering

Formatted: Bullets and Numbering

43. H. Abe , N. Sekimura and T. Tadokoro, Mat. Trans. **46** 433 (2005)

Formatted: Bullets and Numbering

Formatted: Dutch (Belgium)

Tables

$\mathbf{g}\backslash\mathbf{b}$	$\frac{1}{2}[111]$	$\frac{1}{2}[\bar{1}\bar{1}\bar{1}]$	$\frac{1}{2}[\bar{1}\bar{1}1]$	$\frac{1}{2}[1\bar{1}\bar{1}]$	[100]	[010]	[001]
110	1	0	0	1	1	1	0
$\bar{1}\bar{1}0$	0	1	1	0	1	1	0
200	1	1	1	1	2	0	0
020	1	1	1	1	0	2	0

Formatted: Dutch (Belgium)

Table 1: $\mathbf{g}\backslash\mathbf{b}$ table for foil normal $\mathbf{n} = [001]$ for loops of the types expected in Fe and FeCr.

	Ion and T_{irr}	$\frac{1}{2}\langle 111 \rangle$	$\langle 100 \rangle$
Fe	100 keV Fe^+ RT	14%	86%
UHP Fe	150 keV Fe^+ 300°C	10%	90%
Fe9%Cr	30 keV Ga^+ RT	45%	55%
Fe18%Cr	100 keV Fe^+ RT	37%	63%

Deleted: a

Deleted: a

Formatted: Centered

Formatted: Centered

Formatted: Centered

Formatted: Centered

Formatted: Centered

Table 2: Relative proportions of $\frac{1}{2}\langle 111 \rangle$ and $\langle 100 \rangle$ loops in (001) foils.

Deleted: a

Deleted: a

Deleted: [

Deleted:]

For Peer Review Only

UHP Fe irradiated with 150 keV Fe⁺ ions at RT, foil orientation (110), low dose.						
Dose range (counts)	Initial number of loops	Number of initial loops lost	Number of new loops	Number of new loops lost	Total remaining	Comments
4000-4500	10	6	36	12	28	
4500-5000	28	11	28	8	37	2 lost from the initial 10
5000-5500	37	13	20	6	38	None of initial 10 lost
4000-5500	10	8	84	48	38	Summary of data above
UHP Fe irradiated with 150 keV Fe⁺ ions at RT, foil orientation (110), high dose.						
30600-31100	50	10	14	3	51	
31100-31600	51	8	17	4	56	4 lost from initial 50
31600-32100	56	5	8	1	58	2 lost from initial 50
30600-32100	50	16	39	15	58	Summary of data above
UHP Fe irradiated with 150 keV Fe⁺ ions at 300°C, foil orientation (112).						
4000-4500	19	10	37	16	30	
Fe8% Cr irradiated with 150 keV Fe⁺ ions at RT, foil orientation (113).						
4000-5500	34	10	21	4	41	
30600-32100	32	16	32	14	32	2 cases where pairs of loops coalesced
Fe irradiated with 100 keV Xe⁺ ions at RT, foil orientation (113).						
320-640	5	2	54	32	25	
Fe11% Cr irradiated with 100 keV Fe⁺ ions at RT, foil orientation (111).						
800-1600	28	2	80	27	77	2 cases where pairs of loops coalesced
Fe11% Cr irradiated with 100 keV Xe⁺ ions at RT, foil orientation (111).						
80-160	15	0	13	1	27	
240-320	48	10	9	1	46	
Fe11% Cr irradiated with 100 keV Xe⁺ ions at 300°C, foil orientation (111).						
320-640	12	5	28	11	24	

Deleted: [

Deleted:]

Deleted: [

Deleted:]

Deleted: [

Deleted:].

Deleted: [

Deleted:].

Deleted: [

Deleted: ,

Deleted:],

Deleted: see video 7

Deleted: [

Deleted:]

Deleted: , see video 6

Deleted: [

Deleted:],

Deleted: [

Deleted:]

Deleted: , see video 8.

Table 3: Data from dynamic observations of loop loss. Dose conversion: 80 counts = 10¹⁶ ions m⁻²

Material and irradiation condition	1 frame	2 frames	3 frames	4 frames	5 frames	average
Fe11%Cr, 300C 100 keV Xe ⁺		1	3	3	3	3.8
Fe11%Cr, RT 100 keV Xe ⁺	2	5	3			2.1
Fe8%Cr, RT 150 keV Fe ⁺	7	2	1			1.4
Fe(5N), RT 100 keV Xe ⁺		2	2	3	7	4.1
UHP Fe, RT 150 keV Fe ⁺		2	1			2.3

Table 4: Measurements of the time dependence of image contrast for different materials and irradiation conditions. The numbers in each column represent the number of loops which achieved maximum contrast within the given number of video frames. The right hand column gives the average number of frames for maximum contrast to be achieved for that material and irradiation condition. Each frame is equivalent to 1/29th s.

Table to be inserted beneath fig 11.

Total	26	45	50	48
New	26	25	15	13
Lost		6	10	15

For Peer Review Only

Figure captions

Figure 1 Small dislocation loops in (110) UHP Fe and (113) UHP Fe8%Cr irradiated with 150 keV Fe⁺ ions to a dose of $5 \times 10^{17} \text{ m}^{-2}$ ions at RT. The micrographs were taken under weak beam conditions, (g , $\sim 3g$) using the reflection $g = \bar{1}10$.

Figure 2 The density of visible loops per unit area as a function of foil thickness in polycrystalline pure Fe irradiated with 100 keV Fe⁺ at RT. Measurements were made in a wedge-shaped foil imaged under weak-beam conditions using $g = \bar{1}10$ in a foil oriented close to (111) . The foil thickness was estimated by counting thickness fringes, which for the diffraction condition used have a depth periodicity of about 7 nm.

Figure 3 (a) Defect areal densities versus dose for pure Fe. For polycrystalline specimens the approximate orientations of the grains used in the experiments are indicated; the true grain orientations were usually several degrees off the pole. Some representative error bars are shown. Values n of the slopes are shown.
(b) Loop areal densities as a function of dose in FeCr alloys irradiated at RT with 100 keV ions in foils oriented close to (111) .

Figure 4 Areal densities of loops in Fe11%Cr in regions exposed to the 200 kV (sub-threshold) electron beam during 100 keV Xe⁺ ion irradiation compared with regions outside the electron beam. The foil orientation in each case is close to (111) .

Figure 5 Image size distributions of loops in Fe11%Cr produced by irradiation with 100 keV Fe⁺ ions at room temperature (see Figure 2). The ion dose (m^{-2}) and the average loop image diameter are shown above each histogram. Sizes were measured in micrographs with $g = \bar{1}10$ in foils oriented close to (111) .

Figure 6 Loop image size distributions in Fe11%Cr and pure Fe for various irradiation conditions. The average loop image diameter is shown above each histogram. Sizes were measured in micrographs with $g = \bar{1}10$ in foils oriented close to (111) except pure Fe with Xe ions irradiation at RT in foil oriented close to (113) . The dose in each case is $3 \times 10^{17} \text{ m}^{-2}$.

Figure 7 Bright-field kinematical micrographs of single-crystal (001) Fe-9%Cr irradiated in the FIB with 30 keV Ga⁺ ions: (a) $g = 200$, (b) $g = 020$, and (c) $g = 110$. Some loops are ringed for easier identification. The loop which is visible in all three micrographs (dashed circle at top left) has $\mathbf{b} = \frac{1}{2} [1\bar{1}\bar{1}]$ or $\frac{1}{2} [111]$. Those visible only in $g = 200$ and $g = 020$ (solid circles towards the top) have $\mathbf{b} = \frac{1}{2} [\bar{1}11]$ or $\frac{1}{2} [\bar{1}\bar{1}\bar{1}]$. Those visible only in $g = 020$ and $g = 110$ (dotted circles) have $\mathbf{b} = [010]$. Similarly those visible only in $g = 200$ and $g = 110$ (solid circles towards bottom) have $\mathbf{b} = [100]$.

Deleted: ¶

Formatted: Indent: Left: -72 pt

Deleted: UHP Fe and in Fe8%Cr irradiated with 150 keV Fe⁺ ions at RT to a dose ofDeleted: ions m^{-2}

Deleted: .

Deleted: in foils oriented close to (110) and (113) respectively. ¶

Formatted: Font color: Auto

Deleted: .

Formatted: Indent: Left: 0 pt, Hanging: 72 pt

Deleted: The micrograph shows a

Formatted: Font color: Auto

Deleted:), with the foil thickness as shown.¶

Formatted: Font color: Auto

Deleted: ¶

Deleted: .

Formatted: Indent: Hanging: 72 pt

Deleted: ¶

Formatted: Font color: Auto

Deleted: ¶

Formatted: Font color: Auto

Deleted: ¶

Formatted: Font color: Auto

Formatted: Font color: Auto

Deleted: The contrast behaviour allows the loop Burgers vectors to be found. See text for details. ¶

Figure 8 A two-beam dark field $g = 110$ micrograph of loops in single-crystal (111) Fe-11%Cr induced by 30 keV Ga^+ irradiation to a dose of 1×10^{18} ions m^{-2} . The black-white contrast is consistent with first-layer vacancy loops.

Figure 9 (table shown above to be inserted beneath the micrographs) Successive dose increments in Fe-8%Cr irradiated with 100keV Xe^+ ions at RT. The table shows the total number of loops (in a larger area encompassing the area shown), and the number of loops which appeared or disappeared after each dose increment. The foil orientation is close to (111) and $g = \bar{1}10$

Figure 10 Loop number densities as a function of dose in Fe11%Cr irradiated with 100keV Xe^+ ions at RT. (a) in an area with electron illumination and (b) in an area outside the electron beam during ion irradiation. Measurements were made in a foil of orientation close to (111) and $g = \bar{1}10$.

Figure 11 One-dimensional jumping of $\frac{1}{2} \langle 111 \rangle$ loops in UHP Fe in foil orientated close to (112) under electron illumination only: (a) to (d) with the beam focused and showing a range of behaviours of different loops, and (e) showing the same loop as (a) with a defocused electron beam.

Figure 12 (a) Appearance of a new loop in Fe during 100keV Xe^+ irradiation over several frames of a video recording. Each frame is equal to 1/29s. (b) Measurement of the maximum image intensity for the loop shown in (a). This loop took 5 frames from its first appearance to grow to a stable contrast. (c) Another loop in the same material - this loop again took 5 frames from its first appearance to grow to a stable contrast (bottom scale), then suddenly disappeared after 35 frames or nearly 1 second, see top scale. (d) An example of a loop in the Fe-8%Cr alloy which appeared within a single frame. The background intensities shown were measured in the vicinity of the loop in each case. The foils are both orientated close to (113)

Formatted: Font color: Auto

Formatted: Indent: Left: 0 pt, First line: 0 pt

Formatted: Font color: Auto

Formatted: Adjust space between Latin and Asian text, Adjust space between Asian text and numbers

Formatted: Font color: Auto

Formatted: Font: (Default) Times, (Asian) Japanese

Formatted: Font color: Auto

Formatted: Font color: Auto

Deleted: Figure captions¶

¶ Figure 1. Dislocation loops in UHP Fe irradiated with 150 keV Fe^+ ions at 300 °C to a¶ dose of 10^{18} ions m^{-2} , imaged in weak-beam with $g = \bar{1}10$ in a foil with normal close to close to [111]. ¶

¶ Figure 2. TEM weak-beam micrographs of the same area of an Fe11%Cr foil irradiated with 100 keV self-ions at room temperature. Doses are shown above (ions m^{-2}). Weak-beam images with $g = \bar{1}10$. ¶

Figure 3. Comparison of damage in Fe and Fe11%Cr. Weak-beam images using $g = \bar{1}10$ in foils oriented close to (111).

Some of the small loops are ringed. Note the loop density is higher in Fe11%Cr even though the dose is smaller. ¶

Figure 4. The density of visible loops per unit area as a function of foil thickness in polycrystalline pure Fe irradiated with 100 keV Fe^+ at RT. The micrograph shows a wedge-shaped foil imaged under weak-beam conditions using $g = \bar{1}10$, with the foil thickness as shown. ¶

Figure 5(a). Defect areal densities versus dose for pure Fe. For polycrystalline specimens the approximate orientations of the grains used in the experiments are indicated; the true grain orientations were usually several degrees off the pole. Some representative error bars are shown. ¶

□ polycrystalline Hawthorne . (111) 100 keV Fe^+ RT ¶

□ polycrystalline (Kirk *et al.*[38]) . (110) 100 keV Fe^+ RT ¶

⊕ polycrystalline Hawthorne . . (111) 100 keV Xe^+ RT ¶

■ single crystal 4N+ . . (100) 100 keV Fe^+ RT ¶

... [21]

Formatted: Font color: Red

Formatted: Font color: Red

Formatted: Font color: Red

Page 5: [1] Deleted

Mike Jenkins

6/18/2008 4:21:00 PM

There have been a number of studies of damage development in bulk FeCr alloys under neutron irradiation. Gelles [17] carried out neutron irradiations of a range of FeCr alloys (0-12%Cr) at 400°C to 15 displacements per atom (dpa) and found populations of loops, probably of interstitial type, and in most alloys voids. The loops in low (e.g 3%) Cr alloys had predominantly $\langle 100 \rangle$ Burgers vectors, whilst the loops in higher Cr alloys (e.g. 12%) were a mix of $\langle 100 \rangle$ and $\frac{1}{2}\langle 111 \rangle$ types. He suggested that this correlated with the strong swelling suppression of low Cr alloys. Parollo *et al* [18] reported results on neutron irradiations of Fe-Cr alloys with various additions of Cr ranging from 0 to 18%. Specimens were irradiated in bulk at 400°C to doses of 5.5 –7.1 dpa. Again, dislocation loops with Burgers vectors $\langle 100 \rangle$ and $\frac{1}{2}\langle 111 \rangle$ were observed. Cr additions in alloys again resulted in increases in the fractions of loops with $\mathbf{b} = \frac{1}{2}\langle 111 \rangle$. Konobeev *et al* [19] investigated swelling and microstructure of pure Fe and Fe–Cr alloys after neutron irradiation to 26 dpa at 400 °C. The interstitial component of damage was in the form of edge loops with $\mathbf{b} = \langle 100 \rangle$. Voids were also present. More recently Matijasevic and Almazouzi [20] have studied damage development in a range of FeCr alloys and pure Fe under neutron irradiation at 300°C to doses up to 1.5 dpa. Again the damage consisted largely of dislocation loops and both $\langle 100 \rangle$ and $\frac{1}{2}\langle 111 \rangle$ loops were present, although $\langle 100 \rangle$ loops were more numerous. This work is still in progress.

Work has also started on damage development in real ferritic/martensitic steels driven by the potential use of such steels in advanced reactor systems including fusion reactors. For example, Schäublin and Victoria [21] have reported a study of F82H steel irradiated with 590 MeV protons at 40°C to 1.7 dpa and with fast neutrons to doses of 0.5 dpa to 9 dpa at 302°C. In both cases damage was visible in the TEM for doses greater than 0.5 dpa. The damage took the form of small white dots or resolvable loops under weak-beam diffraction conditions. The Burgers vectors of the loops were $\langle 100 \rangle$ and the resolvable loops were analyzed as interstitial type.

Page 7: [2] Deleted

Mike Jenkins

6/3/2008 2:19:00 PM

Figure 2 shows a series of images of the same area of a Fe-11%Cr foil irradiated with 100keV Fe⁺ ions at RT after successive dose increments to the doses shown, taken under similar diffraction conditions as Figure 1. Very few loops are seen at doses $<10^{17}$ ions m⁻². At higher doses loops appear as small white dots of size about 1~3 nm, looking very similar to those seen in Figure 1. However, in like-on-like comparisons (the same type and energy of ion, the same foil orientation and diffraction conditions) the number densities of visible loops were considerably higher in FeCr alloys than in pure Fe, see Figure 3. We now examine this effect quantitatively.

Page 7: [3] Deleted

Jenkins

7/7/2008 3:52:00 PM

The defect yield is then measured as a simple ratio of the loop areal density to the dose.

Page 7: [4] Deleted

Jenkins

7/7/2008 7:22:00 PM

The foil thickness was determined by counting thickness fringes, which for this diffraction condition have a depth periodicity of about 7 nm.

1
2
3 **Page 10: [5] Formatted** **Jenkins** **7/7/2008 4:01:00 PM**

4 Font: Not Bold

5
6 **Page 10: [5] Formatted** **Jenkins** **7/7/2008 4:01:00 PM**

7 Font: Not Bold

8
9 **Page 10: [5] Formatted** **Jenkins** **7/7/2008 4:01:00 PM**

10 Font: Not Bold

11
12 **Page 10: [5] Formatted** **Jenkins** **7/7/2008 4:01:00 PM**

13 Font: Not Bold

14 **Page 10: [6] Deleted** **Jenkins** **7/3/2008 1:20:00 PM**

15 pure

16
17 **Page 10: [6] Deleted** **Jenkins** **7/3/2008 1:20:00 PM**

18 (Hawthorne alloy)

19
20 **Page 10: [7] Deleted** **Jenkins** **7/9/2008 5:12:00 PM**

21 technique of choice to determine the

22
23
24 **Page 10: [7] Deleted** **Jenkins** **7/9/2008 5:12:00 PM**

25 is

26
27
28
29 **Page 10: [7] Deleted** **Jenkins** **7/9/2008 5:13:00 PM**

30 the

31
32
33
34 **Page 10: [7] Deleted** **Jenkins** **7/3/2008 1:23:00 PM**

35 black-white

36
37
38
39 **Page 10: [7] Deleted** **Jenkins** **7/2/2008 10:16:00 PM**

40 black-white

41
42
43
44 **Page 10: [8] Deleted** **Mike Jenkins** **6/18/2008 3:18:00 PM**

45
46 One of the more reliable methods is the so-called black-white contrast technique.
47 Loops lying close to the foil surface may show black-white contrast under two-beam
48 dynamical imaging conditions. If both the sense of the black-white vector \mathbf{l} relative to the
49 diffraction vector \mathbf{g} and the depth of the loop in the layer structure are determined, its
50 nature can be found (see reference [30] for a full discussion). Finding the loop depth by
51 stereo microscopy is difficult and sometimes impossible [32].
52
53
54

55
56 **Page 10: [8] Deleted** **Mike Jenkins** **6/18/2008 3:21:00 PM**

1
2
3 However the analysis may be simplified if there is good confidence that the loop
4 lies in the layer closest to the surface
5
6

7
8 **Page 10: [8] Deleted** **Mike Jenkins** **6/18/2008 3:22:00 PM**

9
10 This first layer
11

12
13 **Page 10: [9] Deleted** **Mike Jenkins** **6/18/2008 3:20:00 PM**

14
15 In our experiments loops were introduced by 30 keV Ga⁺ ion irradiation in a FIB
16 to a dose of 10¹⁸ ions m⁻² at RT. A SRIM calculation [27] showed that in this case the
17 damage peak lies at 6nm and almost all damage lies within about 10 nm of the surface, so
18 that most loops are expected to lie in the first depth layer.
19

20
21 **Page 10: [9] Deleted** **Mike Jenkins** **6/18/2008 2:20:00 PM**

22
23 10
24
25

26
27 **Page 10: [10] Deleted** **Jenkins** **7/2/2008 10:16:00 PM**

28
29 black-white
30

31
32 **Page 10: [10] Deleted** **Jenkins** **7/9/2008 4:01:00 PM**

33
34 .
35

36
37 **Page 10: [11] Deleted** **Jenkins** **7/9/2008 4:01:00 PM**

38
39 Those loops which show black-white contrast
40

41
42 **Page 10: [11] Deleted** **Jenkins** **7/7/2008 4:09:00 PM**

43
44 No loops with $g \cdot l < 0$ are present.
45

46
47 **Page 10: [11] Deleted** **Jenkins** **7/1/2008 6:11:00 PM**

48
49 This experiment does *not* however show that interstitial loops are not also present
50 (see §4.1).
51

52
53 **Page 10: [12] Deleted** **Jenkins** **7/9/2008 4:03:00 PM**

54 It was noticed that loops
55

56
57 **Page 10: [12] Deleted** **Jenkins** **7/7/2008 4:10:00 PM**

58 section
59
60

1
2
3 **Page 14: [13] Deleted** **Jenkins** **7/9/2008 4:18:00 PM**

4 However, with the exception of Fe11%Cr irradiated with 100 keV Xe⁺ ions at RT,
5 there does seem to be a systematic difference between loops produced by Xe⁺ ions and
6 those produced by Fe⁺ ions. In the former case the contrast built up typically over 3-5
7 frames, and there were no examples of a sudden appearance from one frame to the next.
8 In contrast, for Fe⁺ ions the timescale was shorter, typically 1-3 frames. There were
9 several examples of contrast suddenly appearing within a single frame, and none where
10 the contrast built up over more than three frames. In the exceptional case of Fe11%Cr
11 irradiated with 100 keV Xe⁺ ions at RT loops formed within 3 frames: it may be
12 significant that the measurements in this case were made at much lower doses (see § 4.5).
13
14

15 **Page 14: [14] Deleted** **Mike Jenkins** **6/19/2008 10:29:00 AM**

16
17
18
19
20
21
22 **Page 14: [15] Deleted** **Mike Jenkins** **6/18/2008 3:33:00 PM**

23 which show strong black-white contrast

24 **Page 14: [16] Deleted** **Jenkins** **7/9/2008 4:50:00 PM**

25 This conclusion was based on the assumption that the loops showing B-W contrast lay

26 **Page 14: [17] Deleted** **Jenkins** **7/9/2008 5:01:00 PM**

27 , as suggested by SRIM calculations

28 **Page 14: [18] Deleted** **Jenkins** **7/9/2008 4:38:00 PM**

29 However only near-surface loops show

30 **Page 14: [19] Deleted** **Jenkins** **7/9/2008 4:40:00 PM**

31 Further indirect evidence that we are dealing with first-layer loops is provided by the fact
32 that the

33 **Page 16: [20] Deleted** **Jenkins** **7/1/2008 5:01:00 PM**

34 delete

35 This model also provides a possible qualitative explanation of why clustering often
36 occurs over longer time scales in the case of cascades produced by Xe⁺ ions than in
37 cascades produced by Fe⁺ ions. Cascades produced by Xe⁺ ions are expected to be
38 compact with relatively little sub-cascade formation. The diffusion distance L in this case
39 would be the radius of the total cascade. In the case of Fe⁺ irradiation, cascades on
40 average are more diffuse and break up into sub-cascades. We then envisage loop
41 formation to occur when a new *sub-cascade* impinges on a region of high vacancy
42 concentration. The mechanism of loop formation is essentially the same as for Xe⁺ ions –
43 first the formation of a loop nucleus on a very short time scale, followed by accretion of
44 local vacancies by diffusion. However the characteristic diffusion distance L is now the
45 radius of the *sub-cascade*, which on average will be smaller, leading to a shorter diffusion
46 time. In this case loop growth due to diffusion is likely to be more limited, leading to smaller
47 loop sizes in agreement with our observations (Fig. 8).
48
49
50
51
52
53
54

55 We speculate that the exceptional case of Fe11%Cr irradiated with 100 keV Xe⁺
56 ions at room temperature, when loops did not appear over more than 3 time frames, may
57
58
59
60

be related to the low dose at which this measurement was made ($< 5 \times 10^{16}$ ions m^{-2}). At this dose there is only limited cascade overlap. Loops may be produced mostly within individual cascades by the conventional cascade collapse mechanism without the involvement of a background of vacancy clusters, and little thermal diffusion may be involved. All other measurements shown in table 4 were made at doses greater than 10^{17} ions m^{-2} . Further work is in progress to investigate this.

Page 32: [21] Deleted

Mike Jenkins

6/27/2008 11:09:00 AM

Figure captions

Figure 1 Dislocation loops in UHP Fe irradiated with 150 keV Fe^+ ions at 300 °C to a dose of 10^{18} ions m^{-2} , imaged in weak-beam with $g = \bar{1}10$ in a foil with normal close to close to [111].

Figure 2 TEM weak-beam micrographs of the same area of an Fe11%Cr foil irradiated with 100 keV self-ions at room temperature. Doses are shown above (ions m^{-2}). Weak-beam images with $g = \bar{1}10$.

Figure 3 Comparison of damage in Fe and Fe11%Cr. Weak-beam images using $g = \bar{1}10$ in foils oriented close to (111). Some of the small loops are ringed. Note the loop density is higher in Fe11%Cr even though the dose is smaller.

Figure 4 The density of visible loops per unit area as a function of foil thickness in polycrystalline pure Fe irradiated with 100 keV Fe^+ at RT. The micrograph shows a wedge-shaped foil imaged under weak-beam conditions using $g = \bar{1}10$, with the foil thickness as shown.

Figure 5(a) Defect areal densities versus dose for pure Fe. For polycrystalline specimens the approximate orientations of the grains used in the experiments are indicated; the true grain orientations were usually several degrees off the pole. Some representative error bars are shown.

□ polycrystalline Hawthorne	(111) 100 keV Fe^+ RT
□ polycrystalline (Kirk <i>et al.</i> [38])	(110) 100 keV Fe^+ RT
⊕ polycrystalline Hawthorne	(111) 100 keV Xe^+ RT
■ single crystal 4N+	(100) 100 keV Fe^+ RT
⊗ polycrystalline UHP	(110) 150 keV Fe^+ RT
⊖ polycrystalline UHP	(211) 150 keV Fe^+ 300°C
□ polycrystalline UHP	(111) 150 keV Fe^+ 300°C

Figure 5(b) Loop areal densities as a function of dose in FeCr alloys irradiated at RT with 100 keV ions in foils oriented close to (111).

Figure 6 Areal densities of loops in Fe11%Cr in regions exposed to the electron beam during 100 keV ion irradiation compared with regions outside the electron beam.

Figure 7 Image size distributions of loops in Fe11%Cr produced by irradiation with 100 keV Fe^+ ions at room temperature (see Figure 2). The ion dose (m^{-2}) and the average loop image diameter are shown above each histogram.

1
2
3
4 Figure 8 Loop image size distributions in Fe11%Cr and pure Fe for various
5 irradiation conditions. The average loop image diameter is shown above each histogram.
6

7
8 Figure 9 Bright-field kinematical micrographs of FIB-irradiated Fe-9%Cr: (a)
9 $g = 200$, (b) $g = 020$, and (c) $g = 110$. Some loops are ringed for easier identification.
10 The contrast behaviour allows the loop Burgers vectors to be found. See text for details.

11 Figure 10 A two-beam dark field micrograph of loops in Fe-11%Cr induced by FIB
12 irradiation to 1×10^{18} ions m^{-2} . The black-white contrast is consistent with first-layer
13 vacancy loops.
14

15
16
17 Figure 11 (table shown above to be inserted beneath the micrographs)
18 Successive dose increments in Fe-8%Cr irradiated with 100keV Xe^+ ions at RT. The
19 table shows the total number of loops (in a larger area encompassing the area shown), and
20 the number of loops which appeared or disappeared after each dose increment.
21

22
23 Figure 12 Loop number densities as a function of dose in Fe11%Cr irradiated with
24 100keV Xe^+ ions at RT, (a) in an area with electron illumination and (b) in an area
25 outside the electron beam during ion irradiation.
26

27
28 Figure 13 One-dimensional jumping of $\frac{1}{2} \langle 111 \rangle$ loops in UHP Fe under electron
29 illumination only: (a) to (d) with the beam focused and showing a range of behaviours,
30 and (e) showing the same loop as (a) with a defocused electron beam.
31

32
33 Figure 14 (a) Appearance of a new loop in Fe during 100keV Xe^+ irradiation over
34 several frames of a video recording. Each frame is equal to 1/29s. (b) Measurement of the
35 maximum image intensity for the loop shown in (a). This loop took 5 frames from its first
36 appearance to grow to a stable contrast. (c) Another loop in the same material - this loop
37 again took 5 frames from its first appearance to grow to a stable contrast, then suddenly
38 disappeared after nearly 1 second, see top scale. (d) An example of a loop in the Fe-8%Cr
39 alloy which appeared within a single frame. The background intensities shown were
40 measured in the vicinity of the loop in each case.
41
42
43
44
45
46
47
48
49
50
51
52
53
54
55
56
57
58
59
60

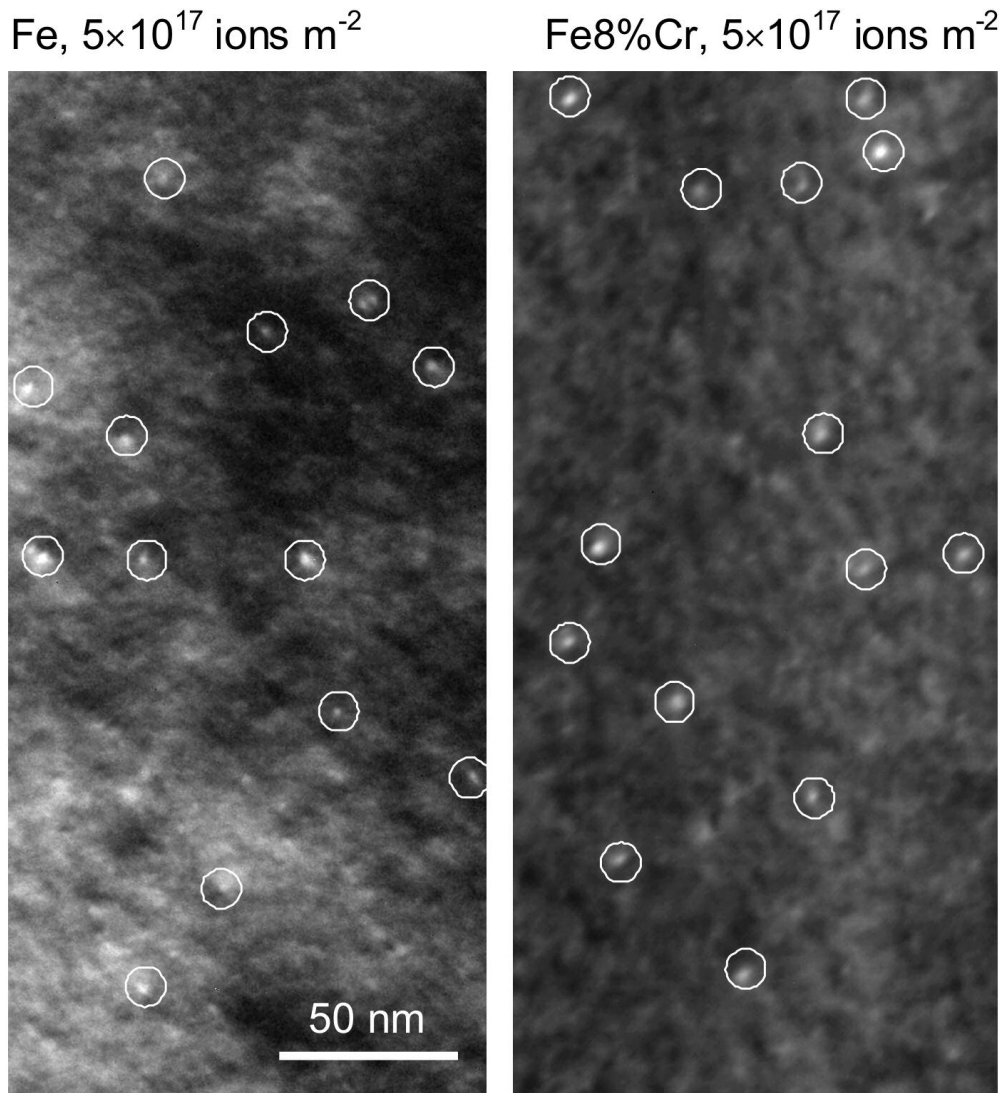


Figure 1



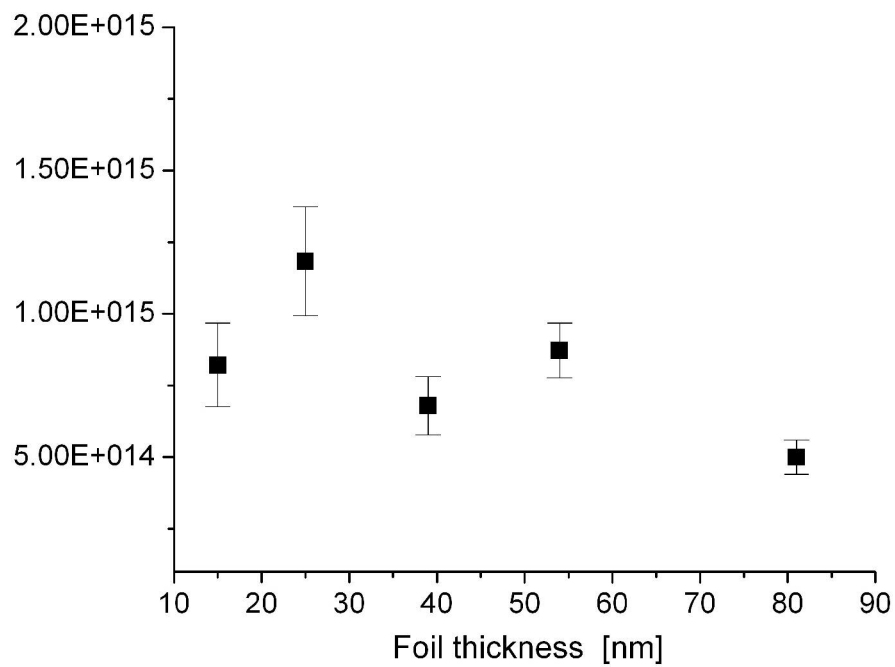


Figure 2
536x416mm (150 x 150 DPI)

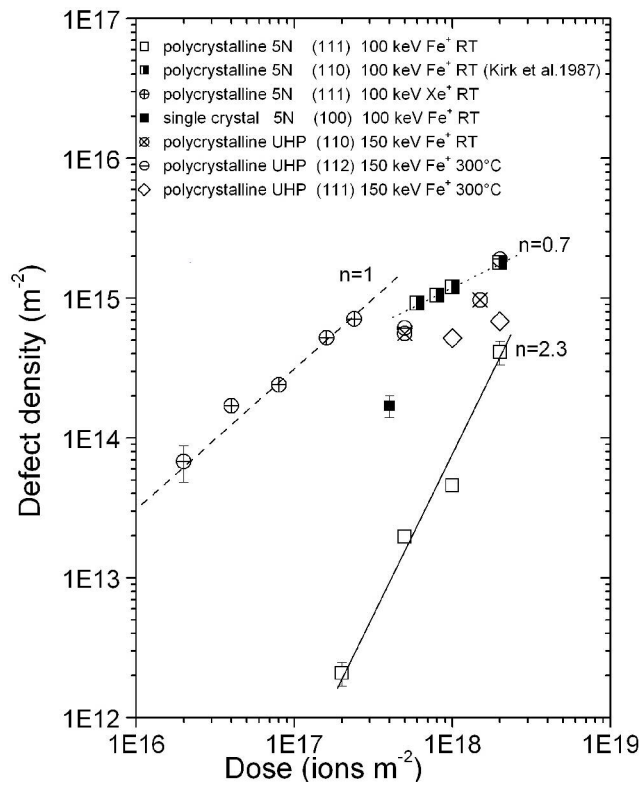


Figure 3a
558x431mm (150 x 150 DPI)

Pre-proof Only

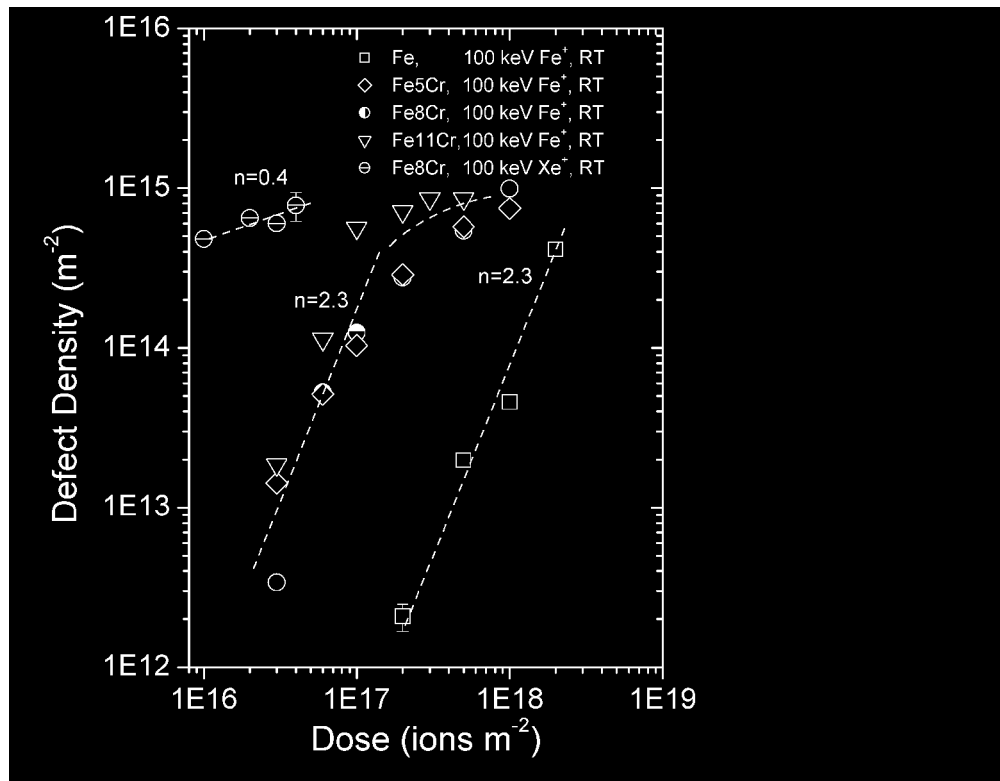


Figure 3b
536x416mm (150 x 150 DPI)

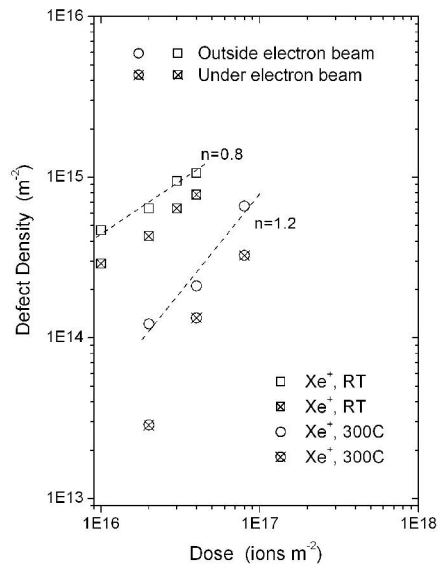


Figure 4
576x403mm (150 x 150 DPI)

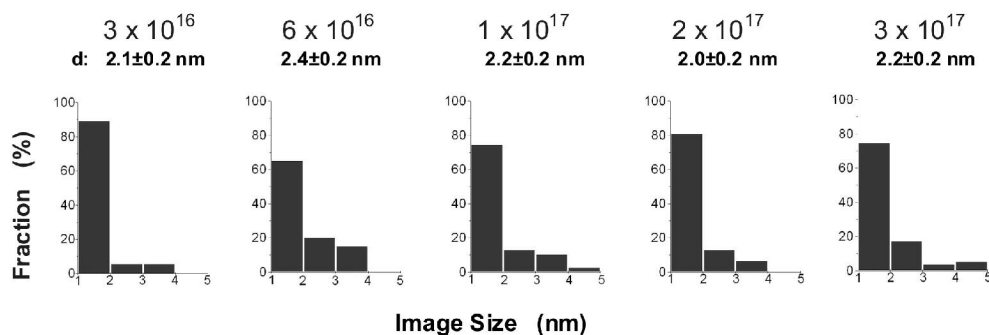
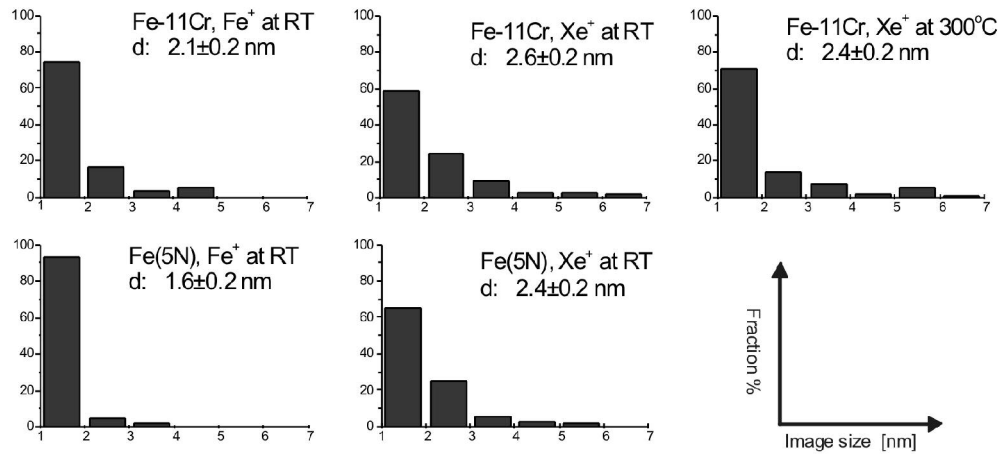


Figure 5

Peer Review Only

1
2
3
4
5
6
7
8
9
10
11
12
13
14
15
16
17
18
19
20
21
22
23
24
25
26
27
28
29
30
31
32
33
34
35
36
37
38
39
40
41
42
43
44
45
46
47
48
49
50
51
52
53
54
55
56
57
58
59
60

**Figure 6**

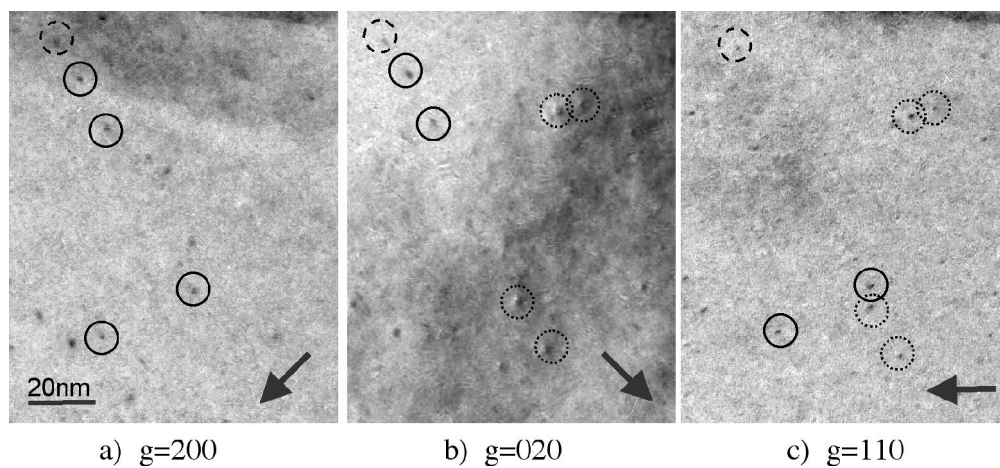


Figure 7
138x63mm (300 x 300 DPI)

1
2
3
4
5
6
7
8
9
10
11
12
13
14
15
16
17
18
19
20
21
22
23
24
25
26
27
28
29
30
31
32
33
34
35
36
37
38
39
40
41
42
43
44
45
46
47
48
49
50
51
52
53
54
55
56
57
58
59
60

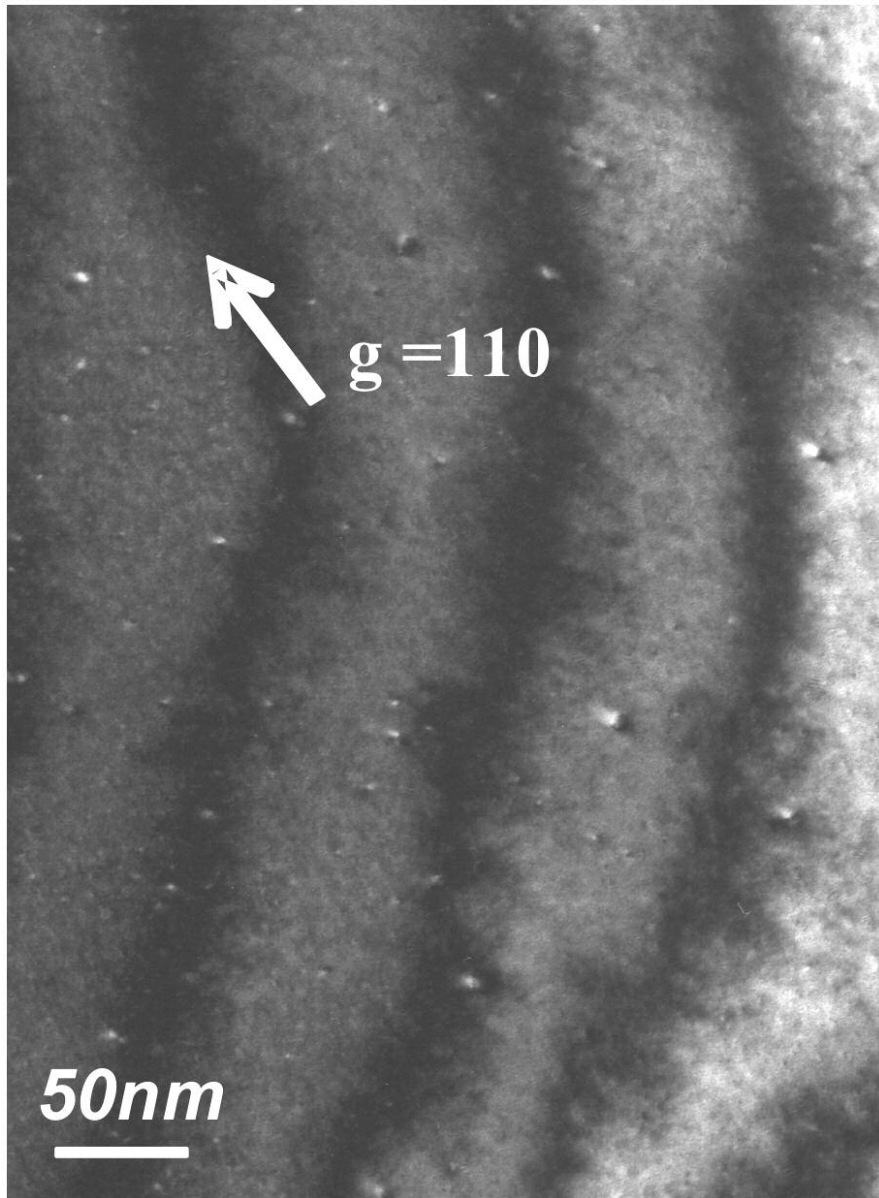


Figure 8

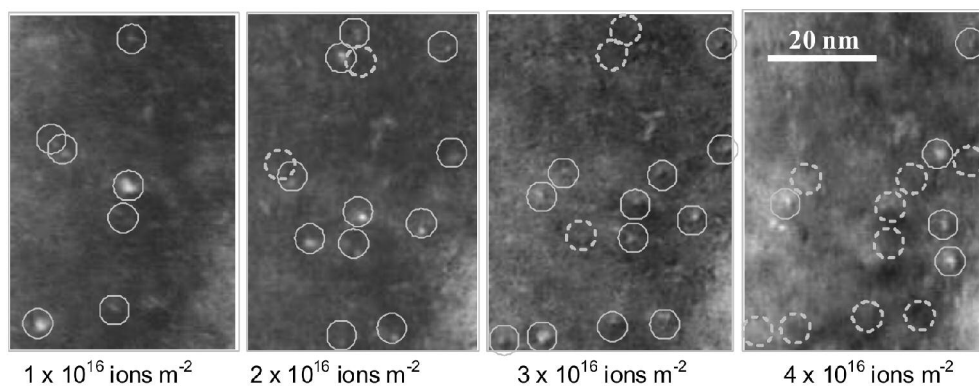


Figure 9

Peer Review Only

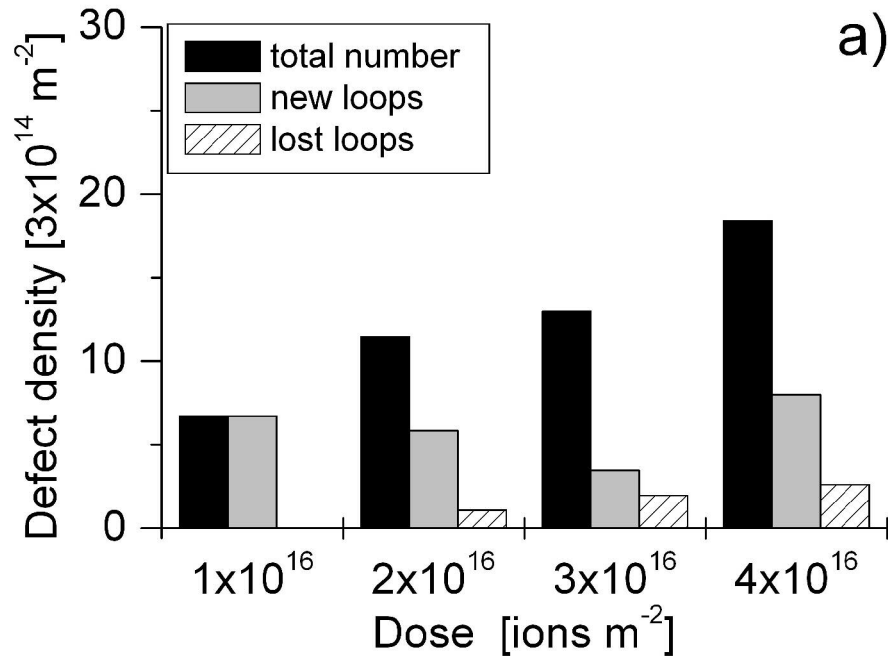


Figure 10a
536x416mm (150 x 150 DPI)

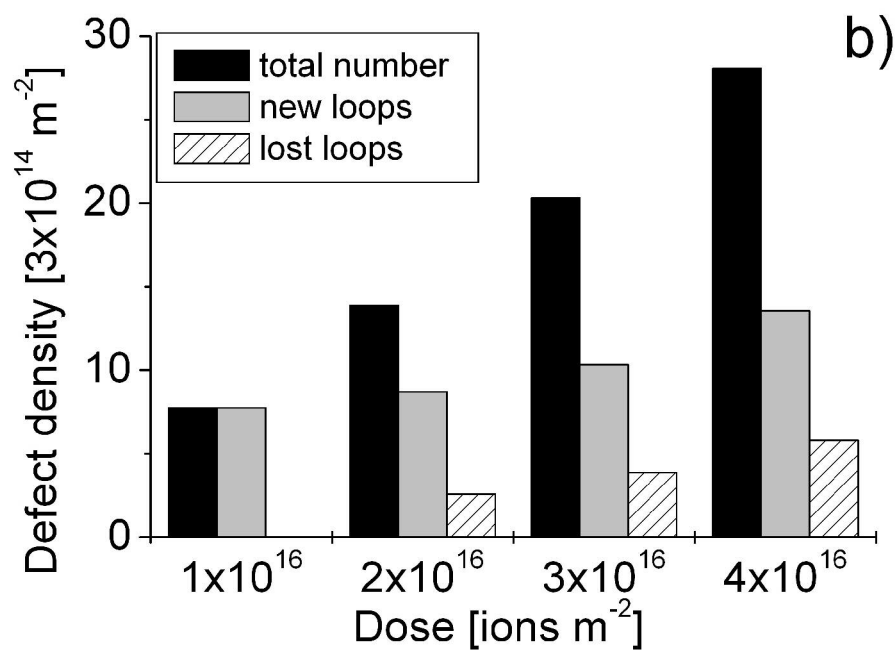


Figure 10b
536x416mm (150 x 150 DPI)

1
2
3
4
5
6
7
8
9
10
11
12
13
14
15
16
17
18
19
20
21
22
23
24
25
26
27
28
29
30
31
32
33
34
35
36
37
38
39
40
41
42
43
44
45
46
47
48
49
50
51
52
53
54
55
56
57
58
59
60

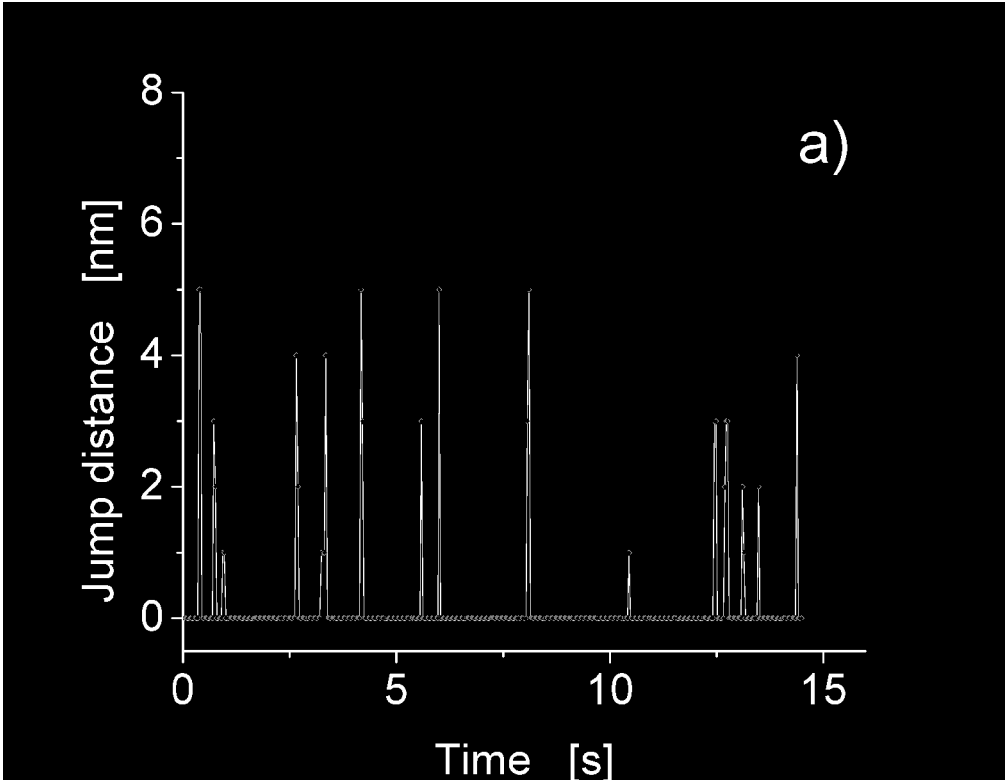
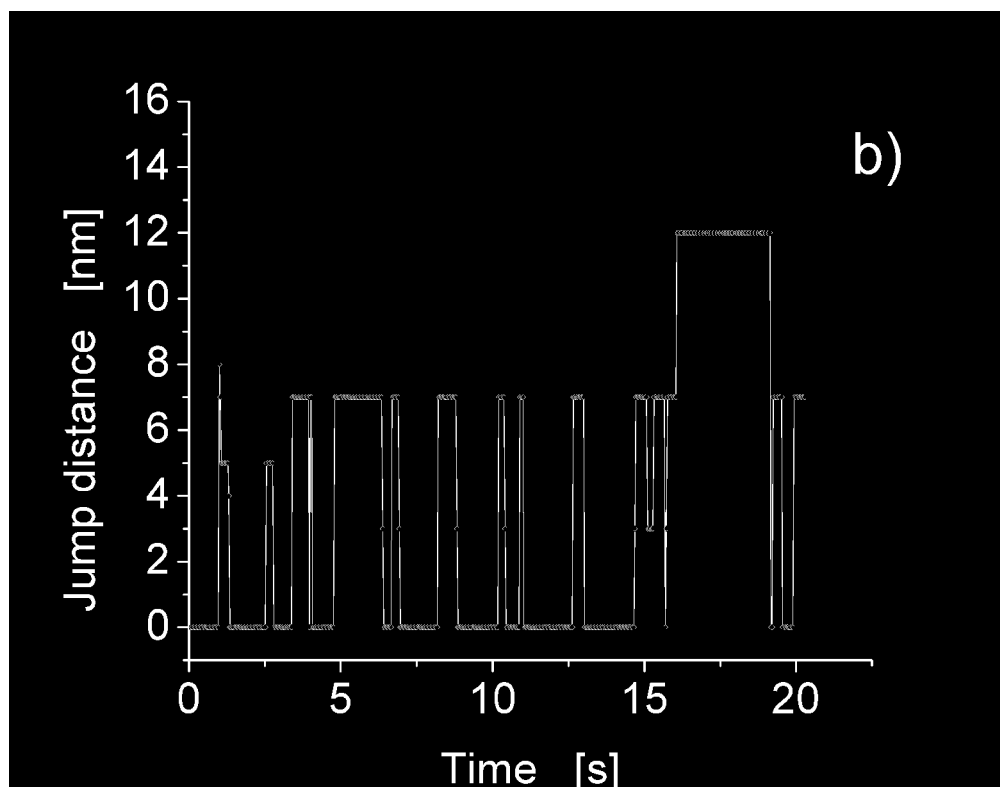


Figure 11a
536x416mm (150 x 150 DPI)

Pre-proof Only

**Figure 11b**

536x416mm (150 x 150 DPI)

1
2
3
4
5
6
7
8
9
10
11
12
13
14
15
16
17
18
19
20
21
22
23
24
25
26
27
28
29
30
31
32
33
34
35
36
37
38
39
40
41
42
43
44
45
46
47
48
49
50
51
52
53
54
55
56
57
58
59
60

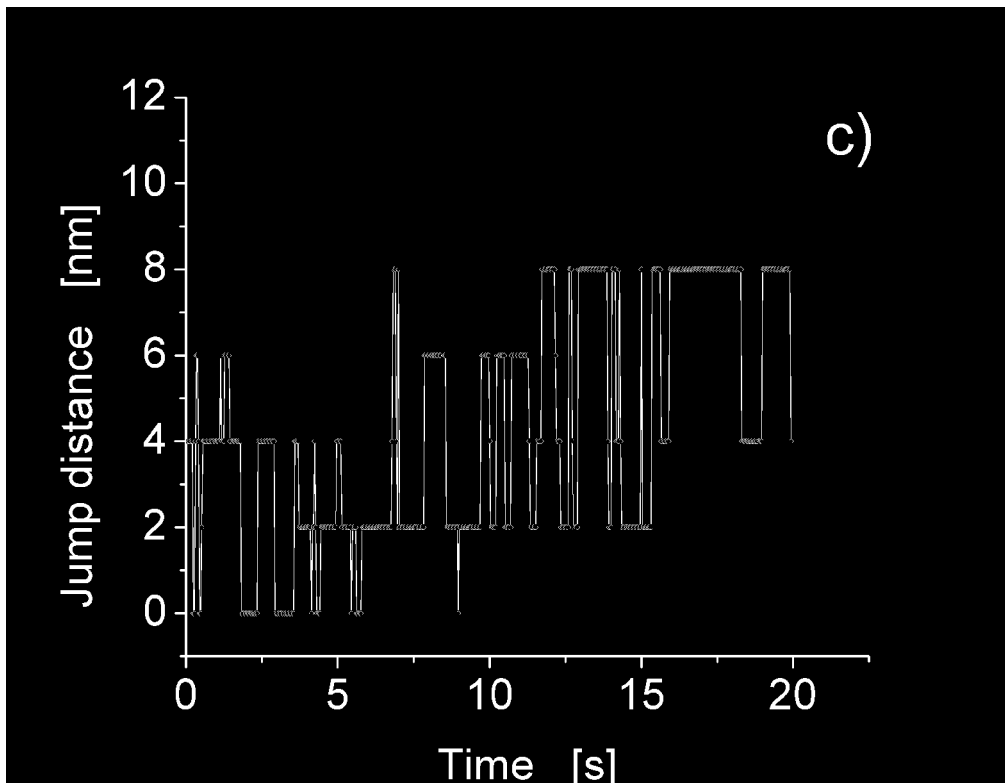
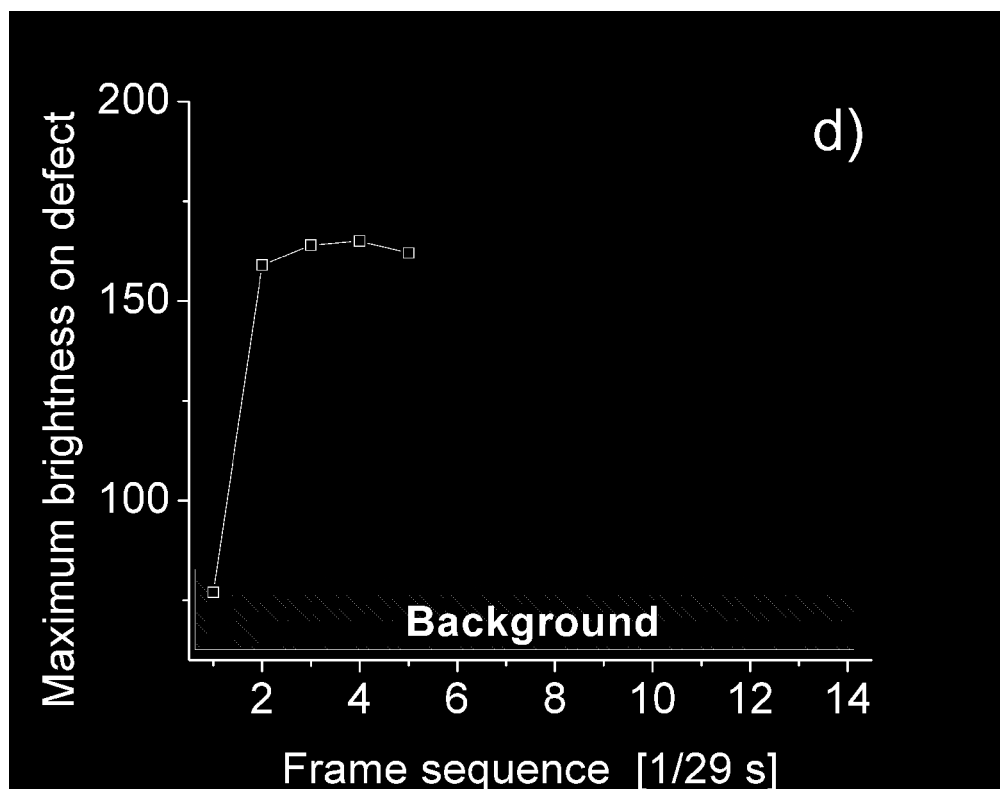


Figure 11c
536x416mm (150 x 150 DPI)

Pre-proof Only

**Figure 12d**

536x416mm (150 x 150 DPI)

1
2
3
4
5
6
7
8
9
10
11
12
13
14
15
16
17
18
19
20
21
22
23
24
25
26
27
28
29
30
31
32
33
34
35
36
37
38
39
40
41
42
43
44
45
46
47
48
49
50
51
52
53
54
55
56
57
58
59
60

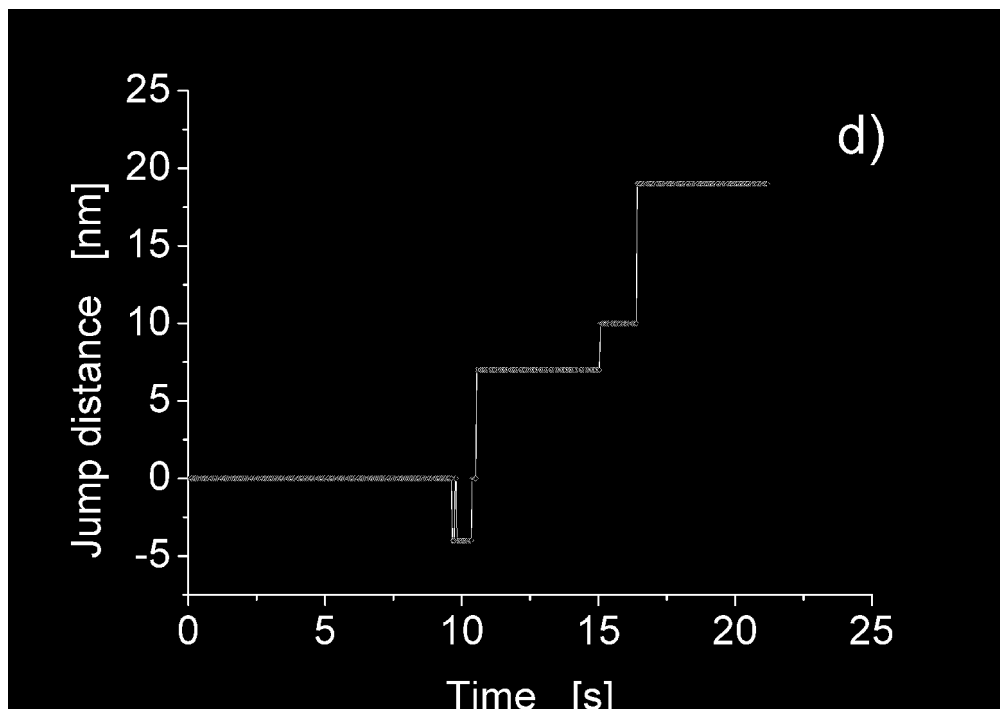


Figure 11d
573x403mm (150 x 150 DPI)

View Only

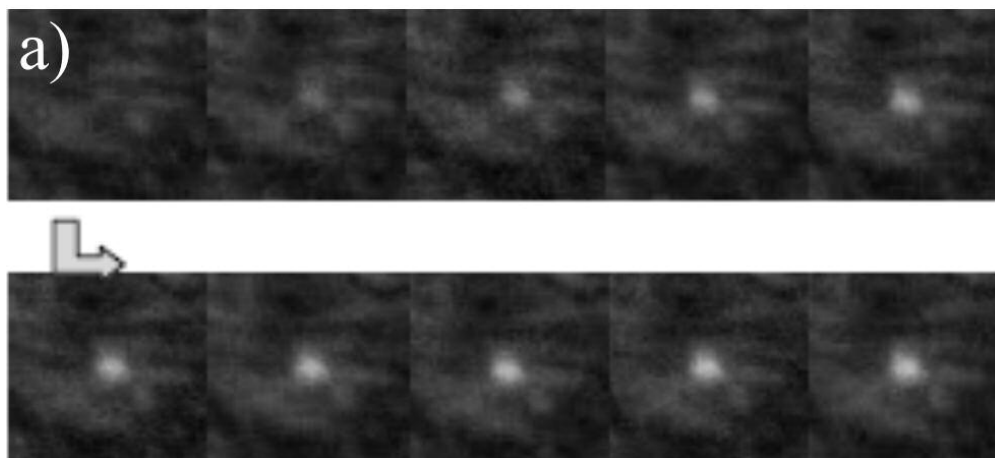


Figure 12a

er Review Only

1
2
3
4
5
6
7
8
9
10
11
12
13
14
15
16
17
18
19
20
21
22
23
24
25
26
27
28
29
30
31
32
33
34
35
36
37
38
39
40
41
42
43
44
45
46
47
48
49
50
51
52
53
54
55
56
57
58
59
60

1
2
3
4
5
6
7
8
9
10
11
12
13
14
15
16
17
18
19
20
21
22
23
24
25
26
27
28
29
30
31
32
33
34
35
36
37
38
39
40
41
42
43
44
45
46
47
48
49
50
51
52
53
54
55
56
57
58
59
60

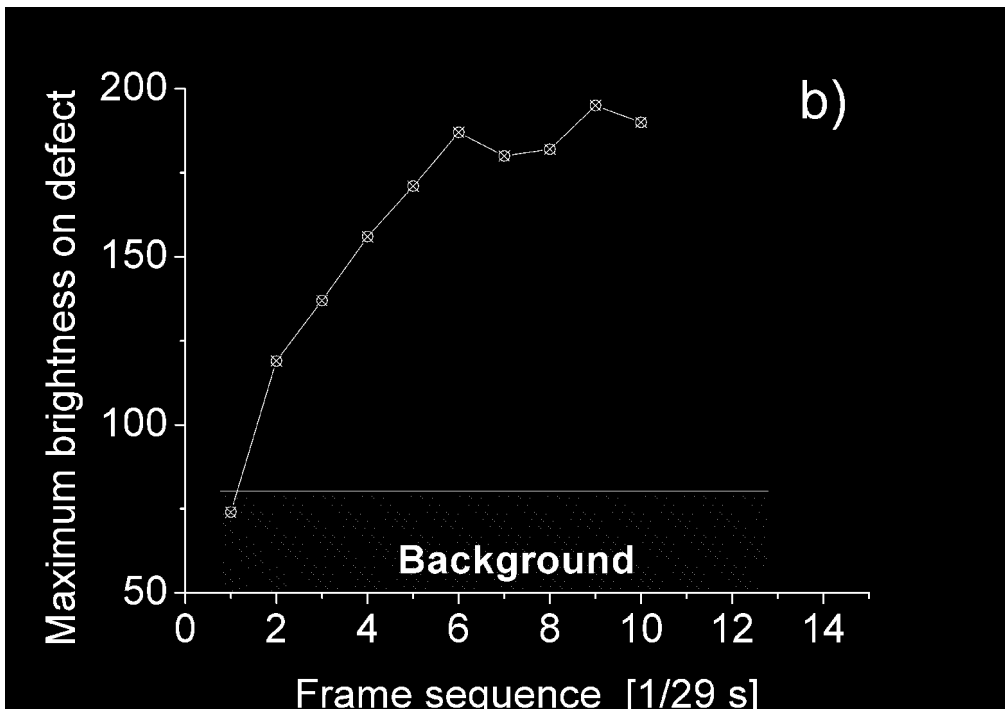


Figure 12b
573x403mm (150 x 150 DPI)

View Only

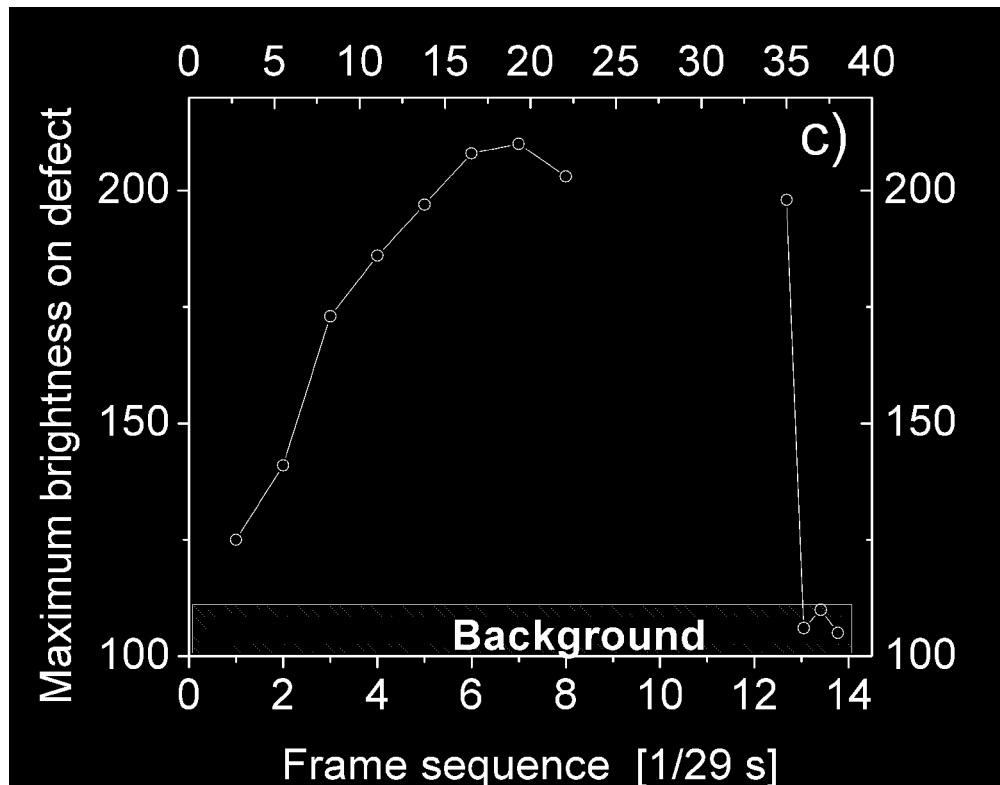


Figure 12c
536x416mm (150 x 150 DPI)

Pre-proof Only